

Spatial heterogeneity of soil organic matter and microbial community composition across ice-wedge polygons and soil layers in Arctic lowland tundra

Victoria Martin^{1,2,3}, Cornelia Rottensteiner^{1,2,3}, Hannes Schmidt¹, Moritz Mohrlok^{1,3}, Julia Horak¹, Carolina Urbina-Malo¹, Julia Wagner^{4,5,6}, Willeke A`Campo⁴, Luca Durstewitz⁴, Niek Jesse Speetjens^{7,8}, Rachele Lodi⁹, Bela Hausmann^{10,11}, Michael Fritz¹², Gustaf Hugelius^{4,5}, Andreas Richter^{1,2}

¹Centre for Microbiology and Environmental Systems Science, University of Vienna, Vienna, Austria

²APRI, Austrian Polar Research Institute

³Doctoral School in Microbiology and Environmental Science, University of Vienna, Vienna, Austria

⁴Department of Physical Geography, Stockholm University, Stockholm, Sweden

⁵Bolin Centre for Climate Research, Stockholm University, Stockholm, Sweden

⁶Department of Ecology and Environmental Science, Umeå University, Umeå, Sweden

⁷Department of Earth and Climate, Vrije Universiteit Amsterdam, Amsterdam, Netherlands

⁸School of Environmental Science, University of Victoria, Victoria, Canada

⁹Institute of Polar Science, National Research Council, Venezia Mestre, Venice, Italy

¹⁰Joint Microbiome Facility of the Medical University of Vienna and the University of Vienna, Vienna, Austria

¹¹Department of Laboratory Medicine, Division of Clinical Microbiology, Medical University of Vienna, Vienna, Austria

¹²Department of Permafrost Research, Alfred Wegener Institute Helmholtz Centre for Polar and Marine Research, AWI, Potsdam, Germany

Correspondence to: Victoria Martin (victoria.sophie.martin@univie.ac.at)

Abstract

Arctic lowland tundra is characterized by pronounced spatial heterogeneity that introduces uncertainty into predictions of permafrost soil carbon dynamics. In these ecosystems, edaphic variability is primarily structured along two spatial axes: ice wedge polygon microtopography at the terrain scale and soil layers at the pedon scale. Here, we investigated how polygon types (low, flat, and high centered polygons) and major soil layers (organic topsoil, mineral subsoil, cryoturbated material, and upper permafrost) jointly shape soil organic matter pools, microbial community composition, and potential extracellular enzyme activities.

Polygon-specific patterns in soil organic matter characteristics and microbial communities persisted across all soil layers, and soil-layer specific differences were consistent across polygon types, while interactive effects were comparatively minor. Low centered polygons showed reduced organic matter bioavailability, lower microbial abundances, and diminished hydrolytic enzyme potential compared to flat- and high-centered polygons. Organic topsoils emerged as pronounced microbial and enzymatic hotspots. The upper permafrost contained substantial

36 amounts of relatively undecomposed organic matter and indicated a considerable potential for hydrolytic
37 degradation upon thaw. Across both spatial axes, patterns in soil organic matter pools, and microbial communities
38 were largely structured along gradients in organic matter inputs and redox conditions, which themselves arise
39 from interactions in surface microtopography, hydrology, and vegetation.

40 Overall, our findings demonstrate that a limited number of spatial units captures a disproportionate share of
41 edaphic, microbial, and biogeochemical variability in Arctic lowland tundra soils. Explicitly accounting for
42 polygon morphologies and major soil layers therefore provides a tractable framework for upscaling soil processes
43 across spatially heterogeneous ecosystems and improving climate-relevant biogeochemical projections.

44 **1 Introduction**

45 Permafrost-affected landscapes are characterized by pronounced surface and sub-surface variability (Ping et al.,
46 2015; Siewert et al., 2021). Over centennial to millennial timescales, periglacial processes have formed a dynamic
47 mosaic of geomorphological landscape features in close spatial proximity (Washburn, 1956). Among the most
48 widespread in continuous permafrost regions are ice-wedge polygons (French, 2007; Washburn, 1973), which
49 cover approximately one third of the Arctic landmass and are particularly prevalent in ground-ice rich lowland
50 tundra and thermokarst terrains of Siberia and North America (Brown, 1967; Fritz et al., 2016). These polygonal
51 networks originate from cyclic freeze–thaw dynamics and repeated frost cracking that promote the formation of
52 ice wedges within the ground (French, 2007; Washburn, 1973). Depending on the state of these ice wedges,
53 distinct polygonal surface patterns eventually emerge through physical self-organization processes (Krantz, 1990;
54 MacKay, 2000). When ice wedges grow, the plastic deformation of overlying soil layers results in elevated rims
55 that enclose lower-lying areas, forming low-centered polygons (LCPs). Conversely, high-centered polygons
56 (HCPs) arise when ice wedges degrade or when sediment or peat accumulation exceeds ice wedge growth,
57 resulting in raised centers surrounded by troughs. LCPs and HCPs thus exhibit inverse topographies (French,
58 2007; Washburn, 1973), whereas so-called flat-centered polygons (FCPs) represent an intergrade type with
59 attributes such as a flat center bordered by shallow drainage channels (Shur et al., 2025, Vaughn and Torn, 2018).

60 In lowland tundra, polygon morphology constitutes a major axis of edaphic variability at the terrain scale. Their
61 microtopographical characteristics influence soil hydrological and thermal dynamics, affect soil type and texture,
62 shape the composition of microbial and vegetational communities, and impact soil biogeochemical processes and
63 the ecosystem energy balance (Lara et al., 2018; Liljedahl et al., 2016; Nitzbon et al., 2019; Wainwright et al.,
64 2015). HCPs typically exhibit well-drained centers with dry surface conditions, whereas the centers of LCPs
65 regularly experience inundation and ponding (Boike et al., 2008; Nitzbon et al., 2019). Waterlogging strongly
66 shapes soil conditions in LCPs. Low oxygen availability restricts microbial decomposition and facilitates organic
67 matter accumulation (Donner et al., 2012; Kuhry et al., 2020), leading to the development of a prominent organic
68 layer (Organic Cryosols). Because wetter soils have higher thermal conductivity, summer active layer depths may
69 reach deeper in LCP centers compared to HCP centers (Liljedahl et al., 2016; Speetjens et al., 2022; Walvoord
70 and Kurylyk, 2016). Yet, soils in LCPs are thought to experience the least pronounced seasonal temperature
71 fluctuations among polygon types (Hubbard et al., 2013), owing to the combined insulating effects of summer
72 inundation, preferential snow accumulation during winter, and peat buildup (Abolt et al., 2018, Grosse et al.,
73 2011). In the less insulated FCPs and HCPs, frost penetrates deeper into the ground, which promotes the mixing

74 of soil layers and leads to the burial of poorly decomposed organic material from the topsoil into the mineral
75 subsoil via cryoturbation (Turbic Cryosoils) (Ping et al., 2008; Wild et al., 2016).

76 Differences in soil properties across polygon types translate into characteristic shifts in plant and microbial
77 community structure and function (Chu et al., 2011; Taş et al., 2018; Wolter et al., 2016). Dry surfaces of HCPs
78 are typically dominated by dwarf-shrubs, forbs, and lichens (Speetjens et al., 2022; Wainwright et al., 2015),
79 whereas vegetation in LCPs is adapted to water-saturated conditions and consists largely of graminoids and peat-
80 or brown-mosses (Minayeva et al., 2018). Gradients in soil redox conditions associated with surface hydrology
81 likewise influence the composition of microbial communities and the dominant pathways of soil organic matter
82 (SOM) transformation (Ernakovich et al., 2017; Liebner et al., 2008; Lipson et al., 2015). Aerobic communities
83 and processes prevail in FCPs and HCPs, whereas anaerobic pathways are common in LCPs (Frank-Fahle et al.,
84 2014; Roy Chowdhury et al., 2021). Because soil physicochemistry, vegetation-derived SOM inputs, and
85 microbial communities jointly regulate biogeochemical cycling (Joabsson and Christensen, 2001; Sachs et al.,
86 2010; Taş et al., 2018; Wallenstein et al., 2007), polygon morphology explains a substantial portion of the spatial
87 variability in lowland tundra carbon exchange (Arora et al., 2019; Wainwright et al., 2015). For example, LCPs
88 are recognized as significant sources of CH₄, whereas CO₂ efflux dominates from HCPs (Lara et al., 2015; Sachs
89 et al., 2010).

90 In permafrost affected systems, another major axis of edaphic variability emerges at the pedon scale (Siewert et
91 al., 2021). Key physicochemical properties such as temperature, redox conditions, ice- and organic matter content,
92 or bulk density show strong vertical stratification along the soil profile. Most notably, the seasonal thaw of the
93 active layer contrasts sharply with the persistently frozen permafrost below. In ice-rich, poorly drained lowland
94 tundra soils, cryogenic processes are especially common. Over time, frost heave and cryoturbation introduce fine-
95 scale irregularities in the vertical arrangement of soil horizons, disrupting the prevailing physicochemical and
96 biotic conditions.

97 Naturally, these gradients and dynamics carry important implications for the life of associated microbial
98 communities. For instance, the permafrost table imposes a strong physical barrier to the exchange of water,
99 nutrients, and gasses between the active layer and the frozen soil (Wilhelm et al., 2011), but also restricts microbial
100 dispersion (Bottos et al., 2018; Doherty et al., 2020; Ernakovich et al., 2022). The position of the permafrost table
101 is, however, temporally variable, and under sustained summer warming the uppermost portion of frozen
102 permafrost (transient layer) may thaw on decadal timescales (Shur et al., 2005). In tundra, topsoil horizons can
103 experience pronounced seasonal and diurnal temperature fluctuations, while deeper horizons remain thermally
104 more stable (Baker et al., 2023; Barbier et al., 2012). Within the active layer, the most marked changes in texture,
105 bulk density, organic matter content, and soil water capacity occur at the transition between the organic topsoil
106 and the mineral subsoil (Alexander, 1989; Bauer, 1974). The influence of plants also decreases rapidly with depth.
107 Approximately 96 % of the root biomass in tundra is concentrated within the upper 30 cm of the soil profile
108 (Iversen et al., 2015; Jackson et al., 1996). Only a few species, e.g., sedges, possess deeper rooting systems that
109 affect deeper layers via oxygenation, exudation, or litter inputs (Joabsson and Christensen, 2001; Shaver et al.,
110 1979). As contributions of acidifying plant-derived inputs such as peat moss biomass and metabolites (Clymo and
111 Hayward, 1982; Jones, 1998; Vives-Peris et al., 2020), or root-derived organic acids diminish with depth, soil pH
112 tends to increase, accordingly. Owing to these depth-dependent patterns, pronounced gradients in the quantity,

113 quality, and stoichiometry of soil organic matter emerge throughout the soil profile (Weintraub and Schimel,
114 2003).

115 Along these two axes of spatial variability a wide range of microbial habitats and ecological niches occurs across
116 comparatively small spatial distances (e.g., Frank-Fahle et al., 2014; Gittel et al., 2014; Malard and Pearce, 2018;
117 Taş et al., 2018). This mosaic of dynamic and contrasting environmental conditions imposes physiological
118 constraints on microbial communities and selects for diverse metabolic strategies and specialized adaptations
119 (Jansson and Taş, 2014; Lipson et al., 2013; Tveit et al., 2013; Waldrop et al., 2025). In frozen permafrost, for
120 example, microbial activity is largely confined to brine-filled channels where liquid water, oxygen, and nutrients
121 are scarce (Ernakovich et al., 2022; Gilichinsky et al., 2003). Active layer horizons and organic topsoils in
122 particular, support substantially higher microbial biomass and diversity (e.g. Doherty et al., 2025; Waldrop et al.,
123 2025), due to less harsh conditions, including greater substrate availability, oxygenation, and hydrological
124 connectivity. The functional and spatial turnover in microbial communities thus links edaphic heterogeneity to
125 microbial metabolic potential and, ultimately, to variability in soil carbon transformations. The production of
126 greenhouse gases through microbial processing of previously frozen organic matter (Graham et al., 2012;
127 Knoblauch et al., 2018; Kwon et al., 2019; Mackelprang et al., 2011; Xue et al., 2016) may shift tundra ecosystems
128 from a net carbon sink to a source (IPCC, 2022; Schuur et al., 2008, 2015b; Voigt et al., 2016). This coupling to
129 the permafrost carbon–climate feedback has made permafrost microbial ecology a central focus of research over
130 recent decades (e.g., Ernakovich et al., 2022; Hultman et al., 2015; Jansson and Taş, 2014; Johnston et al., 2019;
131 Keuper et al., 2020; Waldrop et al., 2023, 2025), yet ecosystem-scale biogeochemical models still inadequately
132 capture the effects of edaphic variability (Sturtevant and Oechel, 2013).

133 We therefore build on a conceptual framework in which different polygon morphologies and soil layers represent
134 the two primary axes of edaphic variability in ice-wedge polygon tundra. Polygon microtopography generates
135 lateral gradients in soil redox conditions, soil types, and organic matter inputs which are associated with distinct
136 hydrologic and vegetation patterns. Vertical gradients along the soil profile impose additional physicochemical
137 controls through shifts in temperature regimes, oxygen availability, pH, and plant inputs. Together, these two
138 spatial dimensions structure organic matter quantity and quality, influence microbial abundance, diversity, and
139 community composition, constrain dominant pathways of organic matter transformation, and shape climate-
140 relevant biogeochemical dynamics. An integrative characterization of polygonal lowland tundra soils across both
141 scales is therefore essential for understanding the functioning of these landscapes and for assessing their future
142 trajectories under climate change. Although effects of polygon morphology on edaphic properties, vegetation, and
143 trace gas exchange have been well described (e.g., Lara et al., 2015; Liljedahl et al., 2016; Sachs et al., 2010;
144 Wainwright et al., 2015), and depth-dependent controls on organic matter composition and microbial communities
145 are also well documented (e.g., (Kuhry et al., 2020; Lynch et al., 2023; Müller et al., 2018; Schnecker et al., 2015;
146 Wild et al., 2016), only few studies have considered both spatial dimensions together (Lipson et al., 2015; Taş et
147 al., 2018).

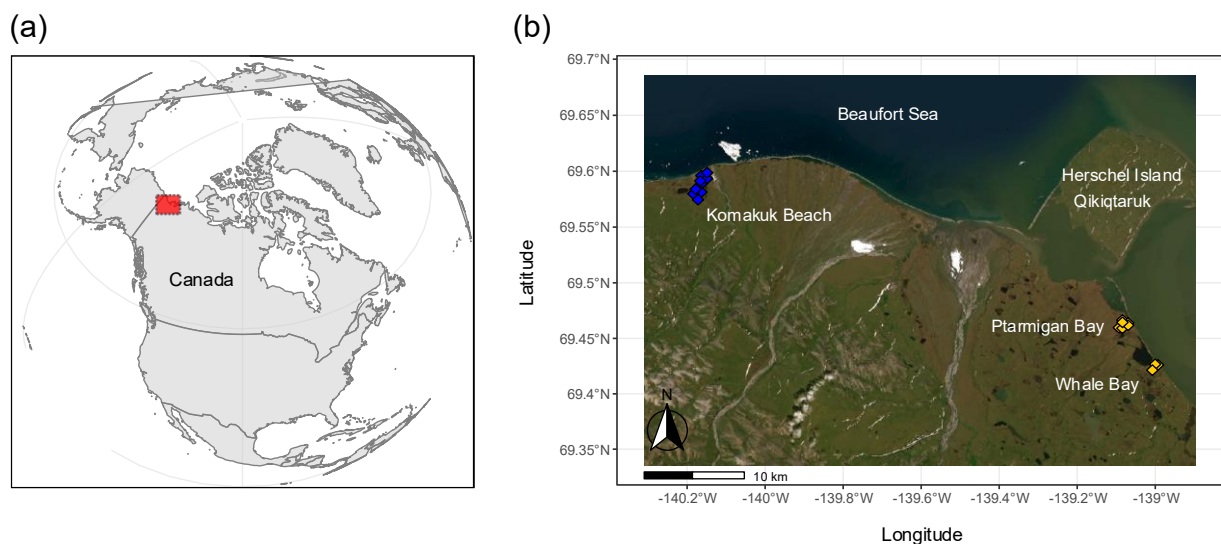
148 To address this gap, we characterized physicochemical properties, organic matter composition, bacterial, archaeal,
149 and fungal community structure, and potential enzyme activities across both axes of edaphic variability in ice-
150 wedge polygon tundra. Specifically, we tested whether (i) polygon morphology (low-, flat-, and high-centered
151 polygons) and soil layers (organic topsoil, mineral subsoil, cryoturbated material, upper permafrost) exert

152 predominantly independent main effects, or interacting controls, and whether (ii) consistent patterns emerge
153 across these scales that may inform scalable representations of Arctic lowland tundra heterogeneity in future
154 ecosystem and land-surface models.

155 2 Materials and Methods

156 2.1 Study area

157 We studied Arctic lowland ice-wedge polygon tundra, located on the coastal plain of the Yukon, Western Canada,
158 (Fig. 1). The first focus area comprised two small lagoons called Ptarmigan Bay ($69^{\circ}27'N$, $139^{\circ}05'W$) and Whale
159 Bay ($69^{\circ}25'N$, $138^{\circ}59'W$). The second focus area, approximately 40 km further towards the west called Komakuk
160 Beach ($69^{\circ}35'N$, $140^{\circ}10'W$), is a small coastal catchment positioned between two alluvial fans. The periglacial
161 landscape in this ecosystem is characterized by a mosaic of ice-wedge polygon networks, mires, beaded streams,
162 and thermokarst lakes (Fritz et al., 2012; Rampton, 1982; Speetjens et al., 2022), underlain by continuous
163 permafrost with a high ground ice content (Couture and Pollard, 2017; Westerveld et al., 2023). The climate is
164 classified as Polar Tundra (Beck et al., 2018), and the vegetation as bioclimatic subzone E/ low Arctic shrub
165 tundra (Walker et al., 2005). Microtopography and relief are strong determinants for the identity of the prevailing
166 soil suborder, and plant species composition. Turbic Cryosols were present in the drier centers of HCPs and FCPs
167 (Canadian System of Soil Classification, Soil Classification Working Group, 1998), where also dwarf-shrubs,
168 forbs, and lichens dominated the flora (Supplementary Table 1(a)). FCPs were mainly characterized by graminoid
169 tussocks and dwarf-shrubs. Inundated centers of LCPs harbored organic Cryosols. The dominant plant groups
170 were graminoids, brown mosses, and peat mosses (Brooks and Lane, 2011; Rampton, 1982; Walker et al., 2005).
171 A more detailed description of the study area, their surface geology, glaciation history, climate, soil suborders and
172 vegetation, can be found in the Supplementary Section 1, and in (Wagner et al., 2023).



173
174 **Figure 1. Study area along the Yukon Coast, Canada (a) and areal overview of the sampling locations (b).** During the
175 2018 field campaign, samples were retrieved from Ptarmigan Bay and Whale Bay (yellow). Komakuk Beach (blue) was
176 investigated during the 2019 field campaign. Maps were created using code available on GitHub (Irwin, 2021). Basemap: (Esri,
177 2024).

178

179 **2.2 Soil sampling and sample storage**

180 Soil sampling was conducted during two field campaigns. Ptarmigan Bay and Whale Bay were sampled in August
181 2018, and Komakuk Beach in August 2019. Sampling took place in late summer, when active layer depths
182 typically approach their seasonal maximum. In the field, we identified larger networks of low-centered (LCP),
183 flat-centered (FCP), and high-centered polygons (HCP) and selected six polygons of each type for sampling
184 (Supplementary Table 1 (a)). For sampling the active layer in HCPs and FCPs, we excavated 1 m – 2.5 m wide
185 soil pits until the permafrost table was reached. We recorded active layer depths, in situ soil temperatures at a
186 distance of 10 cm (Supplementary Table 1(b)), classified soil horizons following Schoeneberger et al. (2012), and
187 documented their distribution and thickness (Supplementary Fig. 1). We collected 100–200 g of fresh material
188 from each horizon by compositing subsamples from several positions within the soil profile. Organic horizons
189 and cryoturbated material were sampled by cutting blocks of known dimensions using a knife. For mineral subsoils
190 we inserted steel cylinders (5.5 cm diameter) horizontally into the exposed profile. Excavating soil pits was not
191 possible for the mostly waterlogged LCPs. We therefore restricted active layer sampling to retrieving two replicate
192 cores per plot using a gas-powered SIPRE corer (diameter 7.5 cm). Documentation, identification and sampling
193 of soil horizons were done in the same manner as described for HCPs and FCPs. In all types of polygons, we
194 sampled the frozen part of the permafrost by using a gas powered SIPRE corer, or by hammering a steel pipe
195 (diameter 4.2 cm) into the ground with a sledgehammer (Hugelius et al., 2010). For each core, we recorded the
196 identity and dimensions of respective horizons and estimated visible ice contents. As within this study only the
197 upper 10 cm of the extracted permafrost cores were used, we strictly refer to the transient layer when discussing
198 characteristics of the permafrost layer.

199 Soil sampling and sample processing followed contamination-minimizing procedures feasible under field
200 conditions: nitrile gloves were worn throughout and changed between samples, tools (e.g., knives, bulk-density
201 cylinders, SIPRE corer) were cleaned with water and sterilized using alcohol-based disinfectant wipes between
202 samples. Permafrost cores were handled on cutting boards lined with fresh aluminum foil, and the outer rind of
203 each core was removed with a sterilized knife before subsampling. Within 24 h after sampling, we carefully
204 removed visible roots, green litter, and coarse solid organic matter fragments from active layer samples and
205 homogenized them by hand. Sample aliquots for DNA extraction were preserved using RNAlater™ Stabilization
206 Solution (ThermoFisher Scientific). Active layer samples were stored and transported at 4 °C, and permafrost
207 samples frozen. The samples arrived approximately two weeks after each respective sampling campaign at the
208 University of Vienna and were processed immediately. Prior analysis, frozen permafrost samples were thawed for
209 two days at 4 °C and homogenized inside the sterile sampling bags. The samples of both field campaigns were
210 treated with the same protocols, analyzed by the same methods and combined into one dataset. For more details
211 see Supplementary Section 1.

212 In total, 81 soil samples were collected (Ptarmigan Bay & Whale Bay n=39; Komakuk Beach n=42). Samples
213 were grouped by polygon type (LCP_n=20, FCP_n=32; HCP_n=29), and by soil layer category (organic
214 topsoil_n=35 including O, Oi, Oe, Oa horizons; mineral subsoil_n=14 including B, Bg horizons, cryoturbated
215 material_n=13 including Ojj, Oijj, Oajj, Ajj horizons, and upper permafrost_n=19 including Off, Bff, Cff
216 horizons). Due to natural heterogeneity in the field and soil-pit specific differences in soil horizon development,
217 an imbalanced sampling design emerged (organic: LCP_n=12, FCP_n=12, HCP_n=11; mineral: LCP_n=2,

218 FCP_n=6, HCP_n=6; cryoturbated: LCP_n=0, FCP_n=7, HCP_n=6; permafrost LCP_n=6, FCP_n=7, HCP_n
219 =6; see also Supplementary Table 1 (c)).

220 **2.3 Physicochemical soil parameters and nutrient pools**

221 The samples were analyzed for bulk density, pH (ultra-clean water), and gravimetric water content (80 °C for 48
222 h). We measured total soil Carbon (Soil C), Nitrogen (Soil N), plus their isotopic composition by an elemental
223 analyzer (EA 1110, CE Instruments, Italy) coupled to a continuous-flow isotope ratio mass spectrometer (IRMS,
224 DeltaPlus, Finnigan MAT). Following a modified ignition method (Kuo, 1996) to convert organic phosphorous
225 (P) to inorganic P, soil total P (Soil P) was determined photometrically in 0.5 M H₂SO₄ extracts via malachite-
226 green-assay (D'Angelo and Crutchfield, 2001). Dissolved organic carbon (DOC) and total dissolved nitrogen
227 (TDN) concentrations were quantified in 1 M KCl extracts via TOC/TN-Analyzer (Shimadzu, TOC-
228 VCPH/CPNTNM-1 analyzer). For more details see Supplementary Section 2, and 10.5281/zenodo.18631833.

229 **2.4 Chemical composition of soil organic matter**

230 The chemical composition of soil organic matter (SOM) was characterized by Pyrolysis-Gas
231 Chromatography/Mass Spectrometry (CDS Pyroprobe 6200, CDS Analytical coupled to Pegasus BT, LECO; with
232 the polar column Supelcowax™ 10 Fused Silica Capillary Column, 30 m x 0.25 mm x 0.25µm film thickness,
233 Sigma Aldrich), using the semi-automated approach that is described in (Martin et al., 2024) with minor
234 modifications. For the qualitative investigation of the SOM pool, we performed Principal Component Analysis
235 (PCA) on center-log-ratio (clr) – transformed abundances (mg C per g soil DW) of 534 pyrolysis products. We
236 further grouped these pyrolysis products into six SOM compound groups (aromatics and phenols, carbohydrates,
237 lignins and lignin-derived compounds, lipids, N-containing substances, compounds of general and unknown
238 origin and explored differences in their absolute and relative abundances among polygon types and soil layer
239 categories. For more details see Supplementary Section 3, and 10.5281/zenodo.18631833.

240 **2.5 Soil microbial communities - DNA extraction, amplicon sequencing, digital droplet (dd)PCR**

241 In this study, microbial ‘communities’ refers to all bacterial, archaeal, and fungal taxa, profiled by amplicon
242 sequencing of the V4 region of the 16S rRNA gene. We extracted microbial DNA (250 mg FW soil from the
243 organic topsoil layer and 400 mg FW soil from all other soil layers) using the FastDNA™ SPIN Kit for Soil (MP
244 Biomedicals, Santa Ana, USA). We followed the manufacturers’ instructions but added minor modifications for
245 the removal of the RNAlater™ Stabilization Solution (addition of 1 ml of provided sodium phosphate buffer to
246 soil pellet, vortex, brief centrifugation, discard supernatant, repeat procedure 5 times). Extraction blanks were
247 included and subjected to subsequent quantification and sequencing steps. Amplicon sequencing and raw data
248 processing was performed at the Joint Microbiome Facility of the Medical University of Vienna and the University
249 of Vienna (JMF project ID JMF-2008-5). A two-step barcoding approach was employed to generate amplicon
250 libraries of archaeal, bacterial, and fungal communities using Illumina MiSeq (V3 Kit, 2 x 300 bp configuration,
251 1 % PhiX spike-in), following Pjevac et al., (2021). We used the primer pairs 515F
252 (GTGYCAGCMGCCGCGGTAA, (Parada et al., 2016) and 806R (GGAACNAGGGTGTCTAAT, (Apprill
253 et al., 2015) for amplifying the V4 hypervariable region of the 16S rRNA gene and the primer pairs ITS1F
254 (CTTGGTCATTTAGAGGAAGTAA, (Smith and Peay, 2014) and ITS2 (GCTGCGTTCTTCATCGATGC,

255 (White et al., 1990) for amplifying the fungal ITS1 region (amplification conditions in Supplementary Section 4).
256 Amplicon pools were extracted from the raw sequencing data using the FASTQ workflow in BaseSpace (Illumina)
257 with default parameters. Demultiplexing was performed with the python package demultiplex (Laros JFJ,
258 github.com/jfjaros/demultiplex), allowing one mismatch for barcodes and two mismatches for linkers and primers
259 (Pjevac et al., 2021). Amplicon sequence variants (ASVs) were inferred using the DADA2 R package applying
260 the recommended workflow (Callahan et al., 2016b, a). FASTQ reads 1 and 2 were trimmed at 150 nt with allowed
261 expected errors of 2 (16S rRNA gene) and 230 nt with allowed expected errors of 4 and 6 (ITS1 region),
262 respectively. Bacterial and archaeal ASV sequences were classified using SINA version 1.6.1 (Pruesse et al.,
263 2012) and the SILVA database SSU RefNR 99 release 138.1 (Quast et al., 2013) using default parameters. Fungal
264 ASVs were classified using DADA2 and the UNITE general FASTA release for eukaryotes (v.8.2), using default
265 parameters (Abarenkov et al., 2020). Datasets were deposited in the NCBI Sequence Read Archive under
266 BioProject accession number (PRJNA1274918).

267 Prior downstream analyses, we cleaned the amplicon sequencing datasets from non-archaeal, -bacterial, or -fungal
268 sequences and excluded samples with less than 500 obtained reads. Contaminant sequences were removed on an
269 ASV-specific basis by subtracting the highest observed read number in one of the DNA extraction blanks from
270 the corresponding sample reads. Rarefaction was applied to these datasets prior to assessing α -diversity (using the
271 `rarefy_even_depth()`-function implemented in `phyloseq` with replacement-argument `==F`; and determined cut-offs
272 at 2650 16S rRNA reads and at 543 ITS1 reads, respectively). We assessed α -diversity as richness (number of
273 observed ASVs) and Shannon diversity.

274 We performed digital droplet PCR (ddPCR) to quantify 16S rRNA genes and ITS1 regions with the same primers
275 used for sequencing. Each ddPCR reaction had a volume of 22 μ L and consisted of 1x QX200 ddPCR EvaGreen
276 Supermix (BioRad), 0.1 μ mol L⁻¹ of each primer and 0.05 and 0.025 ng of template for the quantification of 16S
277 rRNA genes and ITS1 regions, respectively. Droplets were generated on a QX200™ Droplet Generator (BioRad)
278 and directly subjected to PCR amplification (amplification conditions in Supplementary Table 4). PCR products
279 in droplets were kept at 4 °C over night to increase their separation before measuring their fluorescence intensity
280 (on a QX200™ Droplet Reader, BioRad). Gene copy numbers were calculated using the QX ONE Software
281 Standard Edition (v. 1.2, BioRad) where thresholds between positive and negative droplet populations were set
282 consistently for each sample using histograms as a guide. We expressed final ddPCR results as 16S rRNA and
283 ITS1 gene copy numbers g⁻¹ DW soil and used them as abundance proxies for bacteria and archaea, and fungi,
284 respectively.

285 When using the term “absolute abundance” we follow the framework of quantitative microbiome profiling
286 (Vandeputte et al., 2017), in which amplicon-based relative abundances are scaled using gene copy numbers.
287 Accordingly, we calculated ASV-level absolute abundances (gene copy number corrected reads per g soil DW)
288 by multiplying the 16S rRNA or ITS1 gene copy numbers measured in ddPCR assays with their respective relative
289 abundances from the amplicon sequencing datasets (based on the raw reads-dataset after removal of non-archaeal,
290 -bacterial, or -fungal sequences, exclusion of samples with less than 500 obtained reads, and blank-correction).
291 Rare bacterial, archaeal, and fungal taxa (defined as containing less than 0.05 % of all gene copy number corrected
292 reads per sample) were excluded, resulting in 3643 bacterial, 137 archaeal, and 1604 fungal ASVs to be considered
293 in the follow-up analyses. We explored quantitative differences of certain phyla (ddPCR-corrected reads per g

294 DW aggregated on phylum level) between polygon types and soil layer categories. We visualized microbial
295 community composition (β -diversity) by following a widely acknowledged approach for handling compositional
296 data (e.g., Alteio et al., 2021; Barlow et al., 2020; Gloor et al., 2017): Principal Component Analysis (PCA) was
297 performed on center-log-ratio-(clr-) transformed gene copy number corrected reads g-1 DW (corresponding to the
298 ‘Aitchison distance’; Aitchison, 1984) at ASV level. For more details see Supplementary Section 4, and
299 10.5281/zenodo.18631833.

300 **2.6 Microbial extracellular enzymatic activity**

301 We measured the potential activities of six hydrolytic extracellular enzymes involved in carbon-, nitrogen-,
302 phosphorus-, and sulfur-cycling: β -D-1,4-cellobiosidase (exoglucanase), β -D-1,4-glucosidase (glucosidase), β -
303 1,4-N-acetyl-glucosaminidase (exochitinase), acid phosphatase, leucine-aminopeptidase (protease) and sulfatase,
304 using microplate fluorometric assays as described in (Canarini et al., 2021). For more details see Supplementary
305 Section 5

306 **2.7 Statistical analyses and data visualization**

307 All analyses were performed in R Studio Version 4.1.2 (R Core Team, 2017, version 4.1.2). Significances of
308 relationships were tested against a $p < 0.05$ threshold. Plots were generated using ggplot2 (Wickham, 2016) and
309 partly edited using Inkscape (Inkscape, 2020).

310 We employed linear-mixed-effects models (lme) to test all univariate variables for the fixed effects of ‘ice-wedge
311 polygon type’ and ‘soil layer category’ plus their interaction. Therefore, we used the packages lme4 (Bates et al.,
312 2015), lmerTest (Kuznetsova et al., 2017), emmeans (Lenth et al., 2022), and car (Fox and Weisberg, 2019). Due
313 to the sites’ very similar landscape, climate, soil, and vegetation, we determined the random effect in the lme
314 model as specific soil pit ID blocked within the sampling site. Model results were inspected using the anova()
315 function with the default being a type III analysis of variance (ANOVA). In the case of no interactive effect being
316 observed we used type II ANOVA to account for potential effects of different treatment replicates (Langsrud,
317 2003). We used the Estimated Marginal Means post hoc test to perform multiple comparisons ($p.adjust='tukey'$)
318 on the fixed effects of polygon type and soil layer category. In the case of an interactive effect being observed by
319 ANOVA result and /or visual investigation of the data, we compared (a) differences between soil layers per
320 polygon type and (b) differences between polygon types per soil layer category. If homogeneity of variances and
321 normality of model residuals were not given, log or sqrt transformations were applied. In case of no agreement
322 with model assumptions after transformation, we conducted nonparametric tests (for variable-specific details see
323 10.5281/zenodo.18631833). Kruskal Wallis tests were used to test the effects of polygon type and soil layer
324 category, followed by pairwise two-sided Wilcoxon tests (function pairwise.wilcox.test(), $p.adjust='bonferroni'$).
325 To check for possible interactive effects in a comparable manner as described for the lme models, we applied
326 Wilcoxon tests on respectively subsetted parts of the dataset and visually checked the distribution of the examined
327 parameter among the soil layer categories of each polygon type.

328 We employed the phyloseq package (McMurdie and Holmes, 2013) for handling the multivariate datasets on
329 amplicon sequencing and SOM chemical composition. For visualization, we performed Principal Component

330 Analyses (PCAs; function 'phyloseq::ordinate() on centered log-ratio (clr)- normalized data (microbiome::
331 transform(phyloseq.object, "clr").

332 Prior to Permutational Multivariate Analysis of Variance (PERMANOVA) testing, we first checked for
333 homogeneity of multivariate dispersions using Permutation Tests for Multivariate Dispersion Homogeneity
334 (PERMDISP), implemented in vegan (vegan::betadisper() function) with 999 permutations and the argument
335 *bias.adjust = TRUE* to account for unequal sample sizes (Anderson, 2017). Subsequently, we performed
336 PERMANOVAs (on euclidean distances) to explore the effects of polygon type and soil layer category, as well
337 as their possible interaction (adonis() function implemented in vegan with 999 permutations and *p.adjust.m =*
338 *"bonferroni"*, vegan version 2.5-7; Oksanen et al., 2020). Differences between polygon types and/or soil layer
339 categories were assessed using pairwise multilevel comparisons (pairwise.adonis() function implemented in vegan
340 with 999 permutations and *p.adjust.m = "bonferroni"*; Martinez Arbizu, 2020). In case of interactive effects, we
341 used subsetted datasets for making pairwise tests. Analogous to the approach applied for the linear mixed-effects
342 models, we tested (a) differences between soil layers within each polygon type and (b) differences between
343 polygon types within each soil layer. Venn diagrams (get_vennlist(phyloseq.object) were used for visualizing the
344 fraction of shared versus unique pyrolysis products and/or microbial ASVs among polygon types and soil layers
345 respectively (MicrobiotaProcess package, (Xu et al., 2022). We explored potential ecological roles of fungal
346 communities using the FungalTraits database (Pöhlme et al., 2020), with trait-based annotations performed at the
347 genus level. For more details see also Supplementary Section 6, and 10.5281/zenodo.18631833.

348 **3 Results**

349 ***3.1 Physicochemical soil parameters and stoichiometry***

350 We characterized soil properties either by polygon type (averaged across all soil layers) or by soil layer (averaged
351 across all polygon types), respectively. LCPs differed from the other polygon types mainly in their soil C, N, and
352 P contents. Soils of this polygon type had higher C and N concentrations across all layers, whereas P concentration
353 were lower, especially in the organic layer (Supplementary Table 2(a)). Consequently, C:P and N:P ratios were
354 on average double as high in LCP soils compared to FCP or HCP soils. Based on mean values, LCPs were also
355 characterized by the lowest soil bulk density, highest gravimetric soil water content, and deepest active layer
356 among polygon types (Supplementary Tables 1(b), 2(a)), yet these differences were not statistically significant.

357 Physicochemical properties also exhibited pronounced shifts along the soil profile. In situ temperatures decreased
358 steadily from approximately 5.6 °C at the surface to 1.4 °C at the permafrost table (Supplementary Table 1(b)).
359 The strongest contrasts often occurred between organic topsoils and mineral subsoils. For instance, mineral
360 subsoils had a sixfold higher bulk density than the organic layer, but eightfold lower gravimetric water content.
361 Organic topsoils further contained approximately fivefold higher soil C and N contents and twelvefold higher
362 dissolved organic carbon (DOC) and total dissolved nitrogen (TDN) concentrations than mineral subsoils
363 (Supplementary Table 2(b)), whereas cryoturbated material and upper permafrost soils showed intermediate and
364 relatively similar values. Soil C:N ratios remained largely consistent across soil layers, but C:P and N:P ratios
365 were significantly lower in mineral subsoils. The DOC:TDN ratio was nearly twice as high in organic and mineral
366 horizons compared to cryoturbated material and permafrost soils. While soil $\delta^{13}\text{C}$ remained largely stable across

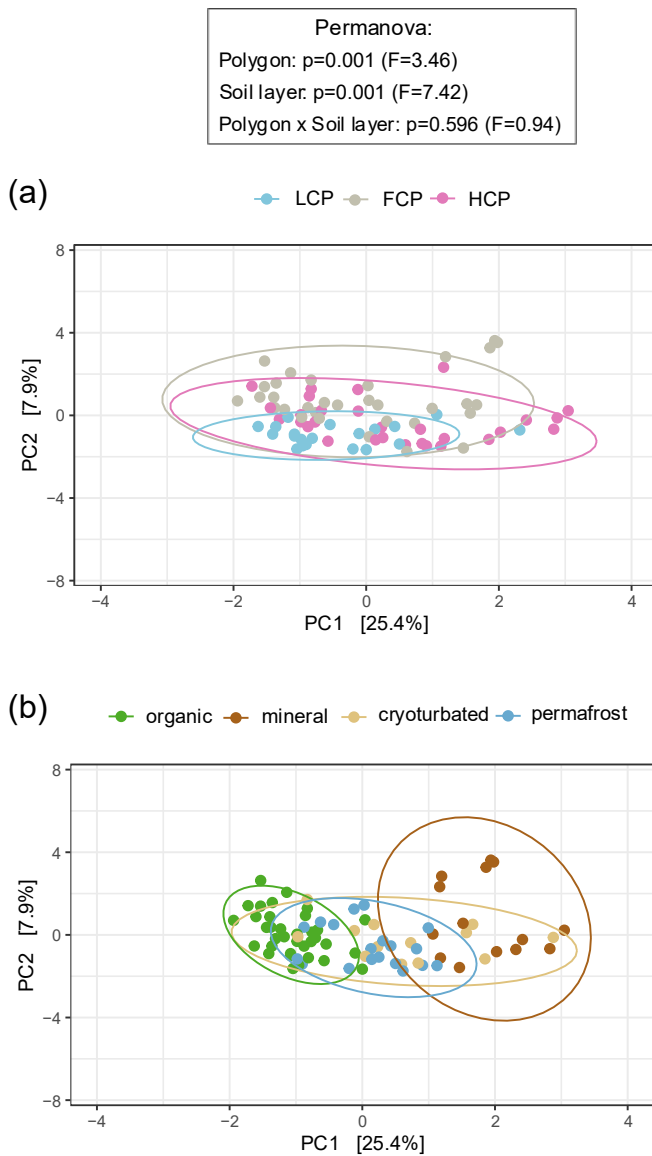
367 layers, soil $\delta^{15}\text{N}$ signals shifted with depth. The organic and mineral layers had more enriched signatures, the
368 permafrost layer more depleted values, and cryoturbated material displayed an intermediate isotopic signature.

369

370 *3.2 Soil organic matter composition*

371 We assessed the chemical composition of organic matter pools in different polygon types and soil layer categories
372 using pyrolysis-GC/MS. We noted a particularly distinct fingerprint pattern of LCP soils, whereas those of FCP
373 and HCP soils were similar (Fig. 2(a)). Correspondingly, LCPs also shared much less pyrolysis products with the
374 other polygon types than were shared among FCPs and HCPs (Supplementary Fig. 2(a)). At the same time, LCP
375 soils also had the smallest fraction of polygon-type specific pyrolysis products. Comparing SOM compound class
376 abundances between polygon types revealed that LCP soils harbored significantly more lignin- derived substances
377 than the other polygon types in absolute and relative terms, and higher absolute abundances of aromatics &
378 phenols, lipids, and general & unknown compounds than FCP soils by trend (Supplementary Fig. 3(a),4(a)).

379 Shifts in the chemical composition of SOM also occurred between soil layers, and this effect was comparatively
380 stronger than the effect of polygon type (Fig. 2(b)). Organic topsoils and mineral subsoils were characterized by
381 rather distinct SOM pools. Their chemical fingerprints differed significantly from those of all other soil layers and
382 included a notable proportion of layer-specific pyrolysis products (10 % and 7 % of all considered pyrolysis
383 products, respectively; Supplementary Fig. 2(b)). The SOM fingerprints from the cryoturbated material and the
384 permafrost layer could not be distinguished from another and only contained a small fraction of unique pyrolysis
385 products (2.5 % of all pyrolysis products, respectively). Absolute abundances of SOM compound groups closely
386 reflected the underlying soil carbon concentrations (Supplementary Table 4). The highest absolute abundances
387 across all six SOM groups were found in the organic topsoil, followed by intermediate levels in cryoturbated and
388 permafrost layers, and the lowest abundances in the mineral subsoil, accordingly (Supplementary Fig. 3(b)). To
389 account for differences in total carbon content, it was hence more suitable to compare the relative abundances of
390 SOM compound classes across soil layers. In relative proportions, aromatic and phenolic compounds were for
391 example highest in mineral subsoils, whilst lowest in organic topsoils (Supplementary Fig. 4 (b)). Similarly, N-
392 containing compounds were most scarce in the mineral layer in absolute terms, while in relative terms,
393 cryoturbated material was the most limited.



394

395 **Figure 2. Soil organic matter (SOM) composition across ice-wedge polygon types (a) and soil layer categories (b).**
 396 Principal component analysis (PCA) was performed on center-log-ratio (clr) -transformed abundances ($\text{mg C g}^{-1} \text{ DW}$) of 534
 397 considered pyrolysis products. PERMANOVA was performed on Euclidean distance matrices, followed by pairwise
 398 PERMANOVA for individual comparisons. Ellipses represent 95% confidence intervals.

399 **(a)** SOM composition differed between polygons, with a distinct fingerprint in LCP soils (LCP vs. FCP: $p = 0.003$, $F = 3.62$;
 400 LCP vs. HCP: $p = 0.018$, $F = 2.87$; FCP vs. HCP: $p = 0.072$, $F = 2.06$). (Betadisper_polygons: $p=0.102$, $F=2.36$; $n_{\text{LCP}}=20$,
 401 $n_{\text{FPT}}=32$, $n_{\text{HCP}}=29$).

402 **(b)** SOM composition differed across soil layers, with distinct fingerprints in organic topsoils and mineral subsoils (organic
 403 vs. mineral: $p=0.006$, $F=17.01$; organic vs. cryoturbated: $p=0.006$, $F=6.43$; organic vs. permafrost: $p=0.006$, $F=5.47$;
 404 mineral vs. cryoturbated: $p=0.012$, $F=3.12$; mineral vs. permafrost: $p=0.006$, $F=7.04$). SOM fingerprints of the
 405 cryoturbated material and permafrost layer could not be distinguished from another ($p=0.252$, $F=1.64$). (Betadisper_soil
 406 layers: $p=0.061$, $F=2.57$; $n_{\text{organic}}=35$; $n_{\text{mineral}}=14$; $n_{\text{cryoturbated}}=13$, $n_{\text{permafrost}}=19$).

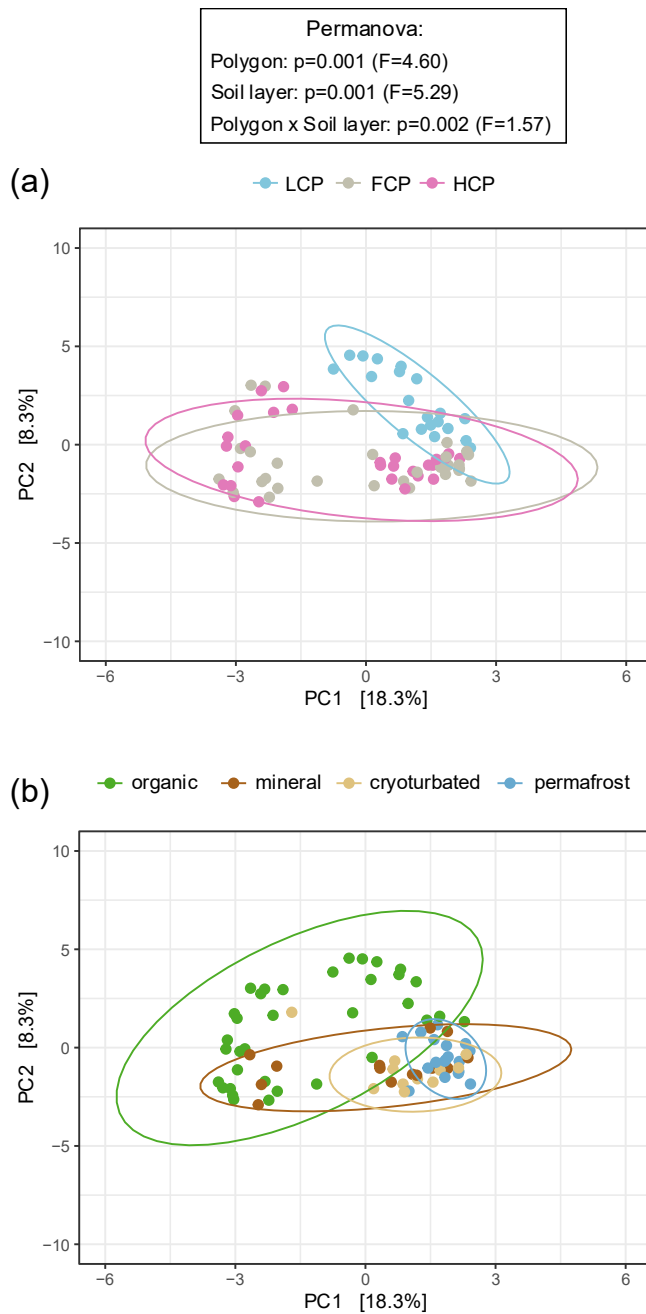
407 **3.3 Microbial Communities**

408 We analyzed microbial community composition by sequencing the bacterial and archaeal 16S rRNA gene and
409 fungal ITS1 region. We used ddPCR derived gene copy numbers to estimate microbial abundances, and to
410 quantitatively assess specific phyla of interest.

411 **3.3.1 Bacterial and archaeal abundance proxies, alpha-, and beta- diversity**

412 The dataset comprised 41 bacterial and six archaeal phyla. Bacteroidota (28.6 %), Proteobacteria (19.8 %),
413 Verrucomicrobiota (16.5 %), Acidobacteriota (14.2 %), and Actinobacteriota (4.5 %), represented the five most
414 abundant phyla, and together accounted for 84 % of all obtained ddPCR-corrected reads. Archaea, by comparison,
415 only comprised 1.8 % of the overall community. Taxonomic resolution was limited for a substantial proportion
416 of the prokaryotic community members, as approximately more than a third (1173 out of 3780) of all bacterial
417 and archaeal ASVs remained unclassified at the family level.

418 Compared to other polygon types, LCP soils exhibited lower richness, Shannon diversity, and reduced abundance
419 of bacteria and archaea (Supplementary Fig. 5). When 16S rRNA gene copy numbers were expressed per gram
420 of dry soil, the lower abundance in LCP soils was only visible in the organic layer (interactive effect). However,
421 when normalized to differences in soil carbon content, bacterial and archaeal abundance was consistently lower
422 across all soil layers of LCPs. The structure of bacterial and archaeal communities in LCP soils also differed
423 significantly from those in FCP and HCP soils (Fig. 3(a)). No significant difference was, however, found between
424 FCP and HCP communities. The distinctiveness of LCP communities was also reflected in other observations.
425 FCPs and HCPs, for example, shared 32 % of the total number of detected ASVs, whereas LCPs shared only 5 %
426 with FCPs, and 2.5 % with HCPs (Supplementary Fig. 6(a)). Furthermore, LCP soils also had the highest
427 proportion of polygon-specific ASVs relative to total ASVs per polygon type (31 % for LCPs, 24 % for FCPs,
428 and 18 % for HCPs), despite harboring a much lower total number of bacterial and archaeal ASVs (1449 for LCPs,
429 2791 for FCPs, and 2471 for HCPs). When comparing absolute abundances patterns across polygon morphologies,
430 we found that three of the five most dominant bacterial phyla, namely Proteobacteria, Verrucomicrobiota, and
431 Actinobacteriota were significantly less abundant in soils of LCPs compared to FCPs and HCPs (Supplementary
432 Table 6, Supplementary Fig. 8). Less abundant compared to either FCPs or HCPs were also Armatimonadota,
433 Bdellovibrionata, Cyanobacterota, and Gemmatimonadota, and phyla, such as RCP2-54, or WPS-2 were nearly
434 absent from LCP soils. By contrast, archaea were notably enriched in LCP soils, particularly in the topsoil layer
435 (Supplementary Fig. 7). LCP topsoils accounted for 65 % of ddPCR corrected archaeal reads in the dataset and
436 were characterized by a high abundance of Euryarchaeota, Crenarchaeota, Micrarchaeota, Nanoarchaeota, and
437 Halobacterota (Supplementary Table 6, Supplementary Fig. 8). This enrichment was evident in relative
438 abundances as well: archaea comprised, on average, 6 % of the total community in LCP topsoils - a substantially
439 higher fraction than in all other soil layers and polygon types. That LCP topsoils harbored particularly distinct
440 communities, was also indicated by the significant interaction between polygon type and soil layer in the
441 ordination (Fig. 3)). For instance, Desulfobacterota (sulfate reducers), and Methyloirabilota (methane
442 oxidizers), occurred in elevated abundances, whereas Acidobacteriota, Myxococcota (predators), and
443 Planctomycetota were comparatively scarce (Supplementary Table 6; Supplementary Fig. 8).



444

445 **Figure 3. Bacterial and archaeal community composition across ice-wedge polygon types (a) and soil layer categories**
 446 **(b).** Principal component analysis (PCA) was performed on center-log-ratio (clr) -transformed abundances (gene copy number
 447 corrected reads g^{-1} DW) of 3780 considered bacterial and archaeal ASVs. PERMANOVA was performed on Euclidean
 448 distance matrices, followed by pairwise PERMANOVA for individual comparisons. Ellipses represent 95% confidence
 449 intervals.

450 **(a)** Bacterial and archaeal community composition differed between polygons, with a distinct fingerprint in LCP soils (LCP
 451 vs. FCP: $p=0.003$, $F=4.76$; LCP vs. HCP: $p=0.003$, $F=5.93$; FCP vs. HCP: $p=0.183$, $F=1.56$). A significant interactive effect
 452 occurred: the LCP organic and permafrost layers hosted unique communities compared to their FCP or HCP counterparts
 453 (statistical details in Supplementary Table 5). Note that heterogeneous dispersions between polygon types may have affected
 454 these results (Betadisper_polygons: $p=0.006$, $F=6.32$; $n_{LCP}=20$, $n_{FPT}=30$, $n_{HCP}=29$).

455 (b) Bacterial and archaeal community composition differed across soil layers, with fingerprints differing between the organic
456 and the permafrost layer in all polygon types (LCP: $p=0.006$, $F=3.37$; FCP: $p=0.006$, $F=4.59$; HCP: $p=0.006$, $F=5.71$). The
457 fingerprints of the cryoturbated material and the mineral layer communities could not be distinguished from another (FCP:
458 $p=0.972$, $F=1.51$; HCP: $p=0.426$, $F=1.31$). A significant interactive effect occurred: in FCPs and HCPs, topsoil and permafrost
459 communities differed from communities of other soil layers in addition (statistical details in Supplementary Table 5). Note
460 that heterogeneous dispersions between soil layers may have affected these results (Betadisper_soil layers: $p=0.001$, $F=31.72$;
461 $n_{\text{organic}}=35$, $n_{\text{mineral}}=14$, $n_{\text{cryoturbated}}=11$, $n_{\text{permafrost}}=19$).

462 Overall, soil layer had a stronger influence on microbial richness, alpha diversity, and abundance patterns than
463 polygon morphology. All metrics declined significantly from the organic topsoil to the permafrost layer
464 (Supplementary Fig.5). For instance, the organic layer harbored twice as many bacterial and archaeal ASVs as the
465 permafrost layer and accounted for 75 % of all 16S rRNA gene copies per gram of dry soil in the dataset (compared
466 to 3.6 % in the mineral subsoil, 11.7 % in cryoturbated material, and 10 % in the permafrost layer). Notably,
467 organic topsoils remained a clear microbial abundance hotspot even after accounting for differences in soil carbon
468 content.

469 Across all polygon types, bacterial and archaeal community structure differed significantly between the organic
470 and permafrost layers, whereas communities in cryoturbated material and adjacent mineral soils were statistically
471 indistinguishable (Fig. 3(b)). The communities in organic topsoils were particularly distinct, with approximately
472 40 % of the total number of bacterial and archaeal ASVs being unique to this layer (mineral layer 5 %, cryoturbated
473 material 2%, and permafrost 3.5 %; Supplementary Fig. 6(b)). The proportion of bacterial and archaeal ASVs that
474 the organic layer shared with other layers declined with increasing soil depth (the organic layer shared 15 % with
475 the mineral, 4 % with the cryoturbated, and 2.5 % with the permafrost layer, respectively). Comparison of absolute
476 phylum-level abundances across soil layers showed that all five most abundant phyla occurred at substantially
477 higher abundances in the organic topsoil than in the permafrost layer (Supplementary Table 6; Supplementary
478 Fig. 8). The phyla that were mostly associated with the permafrost layer were Campylobacterota (93 % of all
479 ddPCR corr. reads assigned to this phylum), Caldisericota (81 %), Cloacimonadota (68 %), and Firmicutes (54
480 %), but also the fraction of unknown taxa was notably high (43 %).

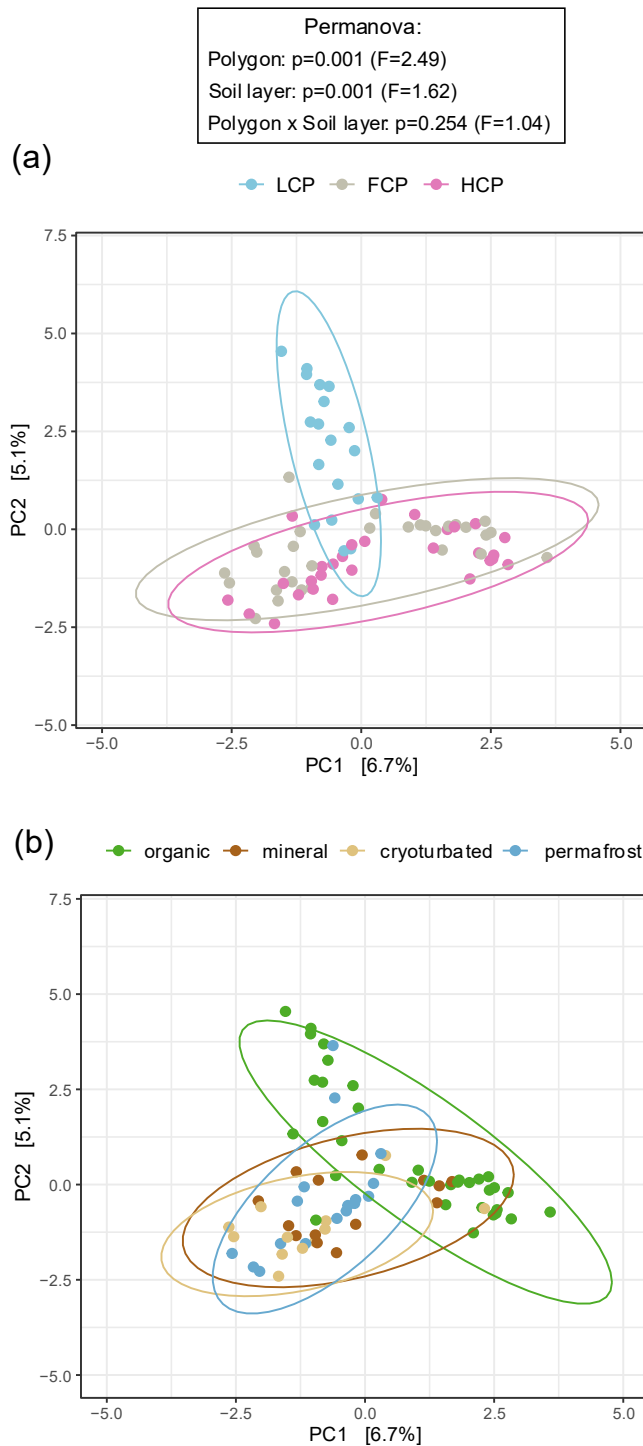
481 *3.3.2 Fungal abundance proxies, alpha-, and beta- diversity*

482 The fungal dataset comprised seven phyla, with Ascomycota and Basidiomycota being the most abundant,
483 together accounting for approximately two thirds of all fungal ddPCR-corrected reads. Taxonomic resolution was
484 limited for a substantial fraction of the dataset. More than 50 % of fungal ASVs (873 of 1604) could not be
485 assigned at the phylum level, representing roughly one third of total fungal reads. Functional annotation using
486 FUNGuild matched ecological roles for approximately 18 % of all fungal ASVs in the dataset, with
487 ectomycorrhizal fungi (6.4 %), saprotrophs (7.7 %, including litter-, wood-, and soil-associated taxa), and root
488 endophytes (1 %) being most prevalent (see also 10.5281/zenodo.18631833).

489 Fungal community patterns largely mirrored those observed for bacteria and archaea. LCP soils showed lower
490 fungal richness, Shannon diversity, and abundances compared to FCPs and HCPs (Supplementary Fig. 9). This
491 lower fungal abundance was restricted to the organic layer when ITS1 gene copy numbers were expressed per
492 gram dry soil (interactive effect) but became evident across all layers after normalization to soil carbon content.

493 Fungal community structure also differed significantly in LCP soils (Fig. 4(a)), with only ~5 % of taxa being
494 shared between LCPs and the other polygon types (Supplementary Fig. 10 (a)). Although LCP soils harbored
495 fewer fungal taxa overall, they contained the highest proportion of polygon-specific ASVs relative to total ASVs
496 (LCPs 60 %, FCPs 55 %, HCPs 53 %). The comparison of phylum-level abundance patterns further supported the
497 presence of less rich, less diverse, and compositionally distinct fungal communities in LCP soils. Compared to
498 FCP and HCP soils, Ascomycota, Basidiomycota, Chytridiomycota, and unclassified fungi occurred in lower
499 abundances, Kickxellomycota were nearly absent, and Mortierellomycota, Rozellomycota and Zoopagomycota
500 were not detected in LCP soils (Supplementary Table 7, Supplementary Fig. 11). Fungal Guilds analysis also
501 suggested that LCP soils harbored a lower range of fungal lifestyles compared to the other polygon types, and that
502 especially the fraction of ectomycorrhizal fungi was smaller.

503 Along the soil profile, fungal richness, diversity, and abundance declined sharply with depth (Supplementary
504 Fig. 9). The vast majority of fungal biomass was concentrated in the organic topsoil, which accounted for 96.2 %
505 of all ITS1 gene copies in the dataset, whereas fungal abundance below the topsoil was minimal (2.4 % in
506 cryoturbated material and <2 % combined in mineral and permafrost layers). Even after normalization to soil
507 carbon content, the organic layer remained a pronounced hotspot for fungal abundance. Also ddPCR derived
508 abundance patterns indicated that all detected fungal phyla occurred in an order of magnitude higher abundance
509 levels in the organic topsoil layer compared to the other layers (Supplementary Table 7, Supplementary Fig. 11).
510 Consistent with this, fungal community structure in organic topsoils was clearly distinct from that in deeper soil
511 layers, independent of polygon type (Fig. 4b). This distinction was further reflected in taxon turnover along the
512 soil profile. Half of all fungal ASVs in the dataset occurred exclusively in the organic layer, and the fraction of
513 shared taxa between the organic layer and other layers also decreased with increasing depth (Supplementary Fig.
514 10 (b)). While all seven fungal phyla were present in the organic layer, six occurred in cryoturbated material, and
515 only four could be detected in the mineral and permafrost layers, respectively (Supplementary Table 7;
516 Supplementary Fig. 11). Fungal Guilds analysis also suggested shifts in fungal lifestyles along the soil profile.
517 The contribution of ectomycorrhizal fungi and root endophytes decreased with depth, while some saprotrophic
518 guilds (i.e., wood and soil saprotrophs) increased slightly.



519

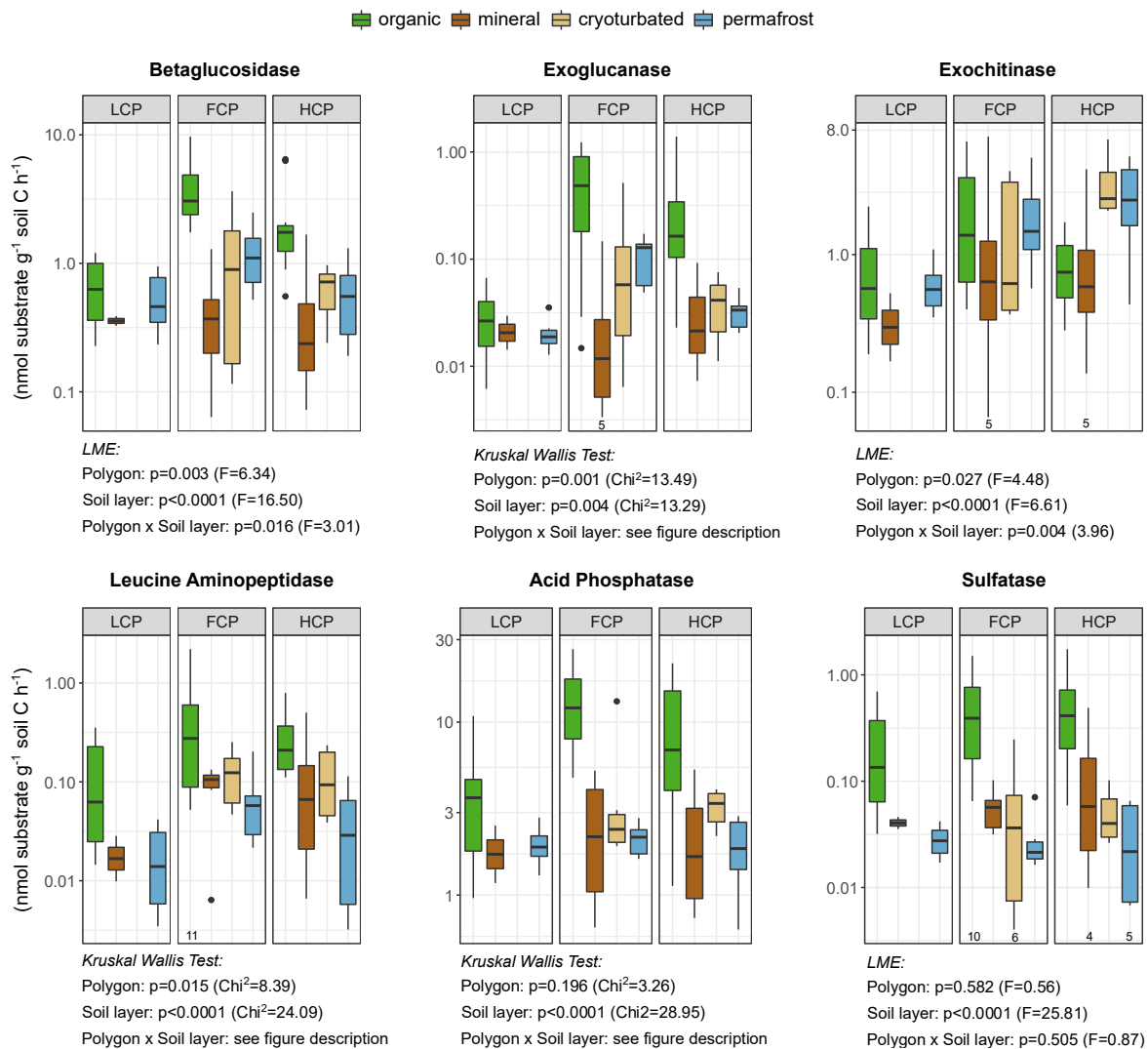
520 **Figure 4. Fungal community composition across ice-wedge polygon types (a) and soil layer categories (b).** Principal
 521 component analysis (PCA) was performed on center-log-ratio (clr)-transformed abundances (gene copy number corrected
 522 reads g^{-1} DW) of 1604 considered fungal ASVs. PERMANOVA was performed on Euclidean distance matrices, followed by
 523 pairwise PERMANOVA for individual comparisons. Ellipses represent 95% confidence intervals.

524 **(a)** Fungal community composition differed across polygons, with a distinct fingerprint in LCP soils (LCP vs. FCP $p = 0.003$,
 525 $F = 2.70$; LCP vs. HCP $p = 0.003$, $F = 3.13$; FCP vs. HCP: $p = 0.009$, $F = 1.72$). Note that inhomogeneous dispersions between
 526 polygon types may have affected these results (Betadisper_polygons: $p = 0.039$, $F = 3.59$; $n_{LCP} = 19$, $n_{FCP} = 30$, $n_{HCP} = 29$).

527 **(b)** Fungal community composition differed between soil layers, with a distinct fingerprint in the organic layer (organic vs.
528 mineral $p=0.024$, $F=1.51$; organic vs. cryoturbated $p=0.006$, $F=2.01$; organic vs. permafrost: $p=0.006$, $F=1.91$). Note that
529 inhomogeneous dispersions between soil layer categories may have affected these results (Betadisper_soil layers: $p=0.003$,
530 $F=5.83$; $n_{\text{organic}}=35$, $n_{\text{mineral}}=14$, $n_{\text{cryoturbated}}=12$, $n_{\text{permafrost}}=17$).

531 *3.4 Potential extracellular enzymatic activity*

532 We expressed enzyme rates per unit of soil carbon to account for a potential effect by diverging soil C
533 concentrations (Supplementary Table 8, Supplementary Fig.12). Overall, potential enzymatic activity per unit soil
534 C varied greater between soil layers than between polygon types (Fig. 5). While activities of P- and S-cycling
535 enzymes did not differ consistently between polygon types, C- and N-cycling enzyme rates were lower in LCP
536 soils compared to FCP and HCP soils. However, this was mainly driven by differences in specific soil layers.
537 LCPs exhibited reduced enzyme activities, with lower rates of betaglucosidase, exoglucanase, and leucine
538 aminopeptidase in the organic layer, and diminished exochitinase activity in the permafrost layer (Supplementary
539 Table 9). Generally, enzyme activity profiles were relatively uniform across soil layers in LCPs but showed
540 pronounced vertical variation in other polygon types. In FCPs and HCPs, activities of betaglucosidase,
541 exoglucanase, and phosphatase still peaked in the organic layer despite normalization to soil carbon. In HCPs,
542 exochitinase activity however reached its maximum in the cryoturbated and permafrost layers, whereas no layer-
543 specific differences occurred in LCPs and FCPs.



544

545 **Figure 5. Extracellular enzymatic activities in investigated soil layer categories and ice-wedge polygon types.**

546 Rates (nmol substrate g⁻¹ soil C h⁻¹) are depicted on a log-scale for improved readability (LCP_organic: n=12, FCP_organic:
 547 n=12, HCP_organic: n=11, LCP_mineral: n=2, FCP_mineral: n=6, HCP_mineral: n=6, FCP_cryoturbated: n=7,
 548 HCP_cryoturbated: n=6, LCP_permafrost: n=6, FCP_permafrost: n=7, HCP_permafrost: n=6; with deviations stated below
 549 respective boxplots). Effects of polygon type and soil layer category are stated under respective panels (LME ANOVA type III
 550 or Kruskal Wallis test results). LCP soils had lower rates of C- and N-cycling enzymes than FCPs and HCP soils. The effect
 551 that was largely driven by soil layer-specific differences (reduced betaglucosidase-, exoglucanase-, leucine-aminopeptidase-
 552 rates in the LCP organic layer, reduced exochitinase rates in the LCP permafrost layer). In LCPs, enzyme activities were also
 553 rather constant across soil layers, but varied considerably in FCPs or HCPs (betaglucosidase, exoglucanase, exochitinase, acid
 554 phosphatase). Statistical details in Supplementary Table 9. Please note that N-, P- and S-depolymerizing enzymes are inherently
 555 related to the C-cycle, which hinders the clear differentiation between microbial nutrient- versus C acquisition.

556 **4 Discussion**

557 In this study, we asked how ice wedge polygon microtopography and soil layers jointly shape soil organic matter
 558 pools and microbial communities, and whether the resulting spatial patterns can guide the upscaling of soil
 559 processes across spatially heterogeneous Arctic lowland tundra ecosystems.

560

561 *4.1 Effects of Polygon Morphology*

562 Across most measured characteristics, FCP and HCP soils were broadly similar, whereas LCP soils consistently
563 stood out as markedly different. This disparity reflects intrinsic features of LCPs, including their distinctive
564 vegetation cover, peaty soils, and persistent summer water saturation. Together, these factors affect a wide range
565 of physical, chemical, and biological processes, and likely shaped the pronounced differences in soil properties,
566 SOM characteristics, and microbial communities observed in this polygon type.

567 Prolonged waterlogging in LCPs strongly restricts microbial decomposition (Dungait et al., 2012; Schädel et al.,
568 2014) and likely contributed to the elevated soil C and N concentrations through the accumulation of plant-derived
569 material. However, for biogeochemical modeling, organic matter quality is considered as important as its quantity
570 (Jansson and Taş, 2014; Mackelprang et al., 2016; Treat et al., 2014). Although soil C:N ratios are used as
571 convenient and easily available proxy for OM availability (Malmer and Holm, 1984; Schädel et al., 2013, 2014;
572 Weiss et al., 2016), they may fail to capture important compositional differences. For our study, we therefore
573 relied on pyrolysis-GC/MS, a method that has been successfully applied in permafrost studies (Folhas et al., 2025;
574 Keskitalo et al., 2021; Verret et al., 2025), and which provides compound-level details that bulk indices like C:N
575 ratios cannot capture. Indeed, soil C:N ratios were similar across polygon types (Supplementary Table 2(b)), but
576 pyrolysis-GC/MS fingerprinting revealed pronounced differences in SOM quality (Fig. 2(a)). LCP soils showed
577 the least variability in SOM composition along both PCA axes and contained the lowest absolute and relative
578 shares of polygon-specific pyrolysis products (Supplementary Fig. 2(a)). This points to a more uniform SOM
579 profile, consistent with the relatively homogeneous nature of graminoid-, or moss-derived peat. In contrast, the
580 more dispersed SOM fingerprints of FCPs and HCPs may reflect their more diverse plant cover and a broader
581 spectrum of litter and root-derived inputs.

582 Beyond vegetation effects, the distinct SOM pattern in LCP soils likely also mirrors the water saturated, low-
583 oxygen conditions that are typical for this polygon type during summer. Being strongly regulated by moisture and
584 oxygen availability (Schmidt et al., 2011; Weintraub and Schimel, 2003), microbial degradation is less efficient
585 under anaerobic than under aerobic conditions (Brune et al., 2000). In anaerobic environments, microbes
586 preferentially consume readily bioavailable substrates, such as carbohydrates and organic acids, while structurally
587 more complex substrates, including long-chained lipids, unsaturated hydrocarbons, lignin, and phenolic
588 compounds tend to accumulate (Tveit et al., 2013, Wilson et al., 2022). Low-oxygen conditions also impede the
589 activity of oxidative enzymes which mediate the breakdown of lignin and phenolic substances (Freeman et al.,
590 2001, 2004; Tveit et al., 2013). Especially in Sphagnum-rich peat soils, these constraints may be further amplified
591 by moss-derived compounds that directly inhibit microbial activity (Fofana et al., 2022; Turetsky, 2003).
592 Together, these mechanisms likely contributed to the elevated relative abundances of lignin-derived compounds,
593 aromatics and phenolics observed in LCP soils (Supplementary Fig. 3(a)).

594 Polygon morphology also strongly influenced microbial abundance, diversity, and enzymatic activity, aligning
595 well with previous reports of distinct microbial communities and metabolic pathways across polygon types (Taş
596 et al., 2018; Wainwright et al., 2015). Although microbial biomass often scales with soil carbon content (Bastida
597 et al., 2021; McGonigle and Turner, 2017), microbial abundance was lowest in the carbon-rich LCP soils, a pattern
598 that even remained after normalizing gene copy numbers to soil carbon content (Supplementary Fig. 5). This

599 strongly indicates that another factor beyond soil carbon acts as overarching force in shaping the LCP microbiome.
600 Redox conditions have been proposed as primary drivers of microbial communities (Lipson et al., 2015) through
601 their influence on oxygen availability, pH, and organic matter quantity and quality. Long-lasting anaerobic
602 conditions as typical for LCP centers, require adapted communities. In our dataset, this is reflected by LCP soils
603 hosting taxonomically distinct communities with minimal overlap with FCP and HCP communities and the
604 highest proportion of polygon-specific taxa (Supplementary Fig. 6(a), 10(a)). Typical of anoxic environments
605 (Lynch et al., 2023), microbial richness and diversity were also lower in LCPs (Supplementary Fig. 5, 9). On the
606 one hand, this likely reflects the scarcity of obligate aerobic taxa. For example, the previously noted enrichment
607 of lignin-derived substances in LCP soils (Supplementary Fig. 3 (a) 4 (a)) corresponds with the low abundance of
608 aerobic, lignin-degrading Basidiomycota (Supplementary Table 7; Supplementary Fig. 11), (Zak and Kling, 2006).
609 On the other hand, anaerobic metabolic pathways such as fermentation, methanotrophy, and respiration via
610 alternative electron acceptors yield less energy than aerobic respiration (Madigan et al., 2021), which may
611 constrain microbial growth yields and the number of organisms that can be sustained. Archaea likely contributed
612 disproportionately to the distinct prokaryotic community structure of LCP soils (Fig. 3(a)). Although archaea
613 generally represent a minor fraction of Arctic soil microbiomes (Gittel et al., 2014; Müller et al., 2018; Wilhelm
614 et al., 2011), they can become prominent in waterlogged and peaty soils. In our dataset, archaea accounted for just
615 1.8 % of all prokaryotic ddPCR-corrected reads overall, but were strongly enriched in LCP soils (7.3 %) compared
616 to FCP (1.2 %) and HCP (0.2 %) soils (Supplementary Fig. 7). Notably, Crenarchaeota and Euryarchaeota were
617 particularly enriched in LCP soils (Supplementary Table 6; Supplementary Fig. 8), phyla that include taxa
618 involved in key peatland biogeochemical processes such as methanogenesis and anaerobic methane cycling. (Tveit
619 et al., 2013). Beyond the briefly noted influence of redox conditions, the distinct fungal community fingerprint
620 observed in LCP soils (Fig. 4a) is likely driven by differences in plant species composition (Chu et al., 2011;
621 Malard and Pearce, 2018; Wallenstein et al., 2007). For instance, LCPs are dominated by sedges and mosses (e.g.,
622 *Eriophorum* sp., Sphagnaceae, Amblystegiaceae), which typically lack mycorrhizal associations (Chen et al.,
623 2020), whereas FCPs and HCPs are richer in dwarf shrubs (e.g., *Betula*, *Salix*, Ericaceae) that form mycorrhizal
624 symbioses (Lynch et al., 2018). Consistent with these vegetation differences, the relative abundance of
625 ectomycorrhizal fungi was substantially lower in LCP soils (2.2 %) than in FCP (7.8 %) and HCP (6.8 %) soils
626 (FUNGuild analysis, Supplementary dataset 3)).

627 Finally, polygon-specific differences in microbial communities and SOM characteristics were mirrored in
628 extracellular enzyme activities. Heterotrophic microbes rely on extracellular enzymes to depolymerize high-
629 molecular-weight substrates, with enzyme production regulated by substrate availability and microbial demand
630 (Burns et al., 2013; Moorhead et al., 2012). Accordingly, the lower potential activity of hydrolytic C- and N-
631 acquiring enzymes in LCP soils, and particularly in the organic layer (Fig. 5), corresponds well with the detected
632 lower microbial abundance and diversity and the pronounced depletion of (Supplementary Fig 5, 9). Fungi are
633 key decomposers, producing a wide suite of hydrolytic and oxidative enzymes (Baldrian et al., 2010; Schneider
634 et al., 2012). In high-latitude ecosystems, mycorrhizal fungi play a vital role for hydrolytic protein degradation
635 (Bending and Read, 1996; Read and Perez-Moreno, 2003), while white-rot fungi, such as Basidiomycota,
636 oxidatively degrade lignin and humified SOM (Hatakka, 2005; Lee et al., 2012b). Both groups, however, occurred
637 in low abundances in LCP soils (Supplementary Table 7, Supplementary Fig. 11, FUNGuild analysis). Although
638 our assays targeted only hydrolytic enzymes, the accumulation of lignin and phenolic compounds in LCP soils

639 (Supplementary Fig. 3(a)) suggests that oxidative enzyme activity was suppressed too, likely as a consequence of
640 low-oxygen conditions (Freeman et al., 2004; Tveit et al., 2013). Elevated concentrations of polyphenols may
641 further reinforce this pattern by exerting negative feedback on enzyme activity (Kostka et al., 2016). Finally,
642 because enzyme production is energetically costly (Wortel et al., 2018), aerobic communities in FCPs and HCPs
643 may be able to allocate more energy toward enzyme synthesis than the predominantly anaerobic communities in
644 LCPs.

645 *4.2 Effects of Soil Layer*

646
647 While LCP soils consistently differed from FCP and HCP soils, soil-layer effects were more nuanced, with each
648 layer exhibiting characteristic features. We advocate that many of the observed patterns can be interpreted along
649 gradients in redox conditions, SOM content, or their interplay. Soil pH, for example, was consistently lower in
650 organic topsoils than in the permafrost layer (Supplementary Table 2(b)), a pattern also reported by Gentsch et
651 al., (2018). This contrast suggests that the dominant controls on soil pH vary with depth, even though both layers
652 may experience oxygen-limitations at times. In the permafrost layer, inorganic redox reactions and proton-
653 consuming microbial processes (e.g., iron-, manganese-, sulfate-, or nitrate reduction) likely exert a strong
654 influence on soil pH. Contrastingly, pH in the topsoil layer is more strongly shaped by acidifying plant inputs,
655 including organic acids released as root exudates (Vives-Peris et al., 2020), or Sphagnum mosses, which acidify
656 their surrounding via their metabolism and galacturonic acid-rich biomass (Kostka et al., 2016).

657 Broad-scale indicators for SOM composition and degree of processing, such as bulk soil C:N ratios and $\delta^{13}\text{C}$
658 signatures remained remarkably stable across soil layers, (Supplementary Table 2(b)), likely due to extensive
659 cryoturbation activity in the study area. However, finer-scale changes in SOM quality became evident from the
660 pyrolysis-GC/MS analysis. The ordination pattern (Fig. 2(b)) revealed a pronounced compositional shift along the
661 first PCA axis that closely mirrored the concomitant gradient in soil carbon content (two-sided Spearman rank
662 order correlation: Soil C - PCA axis 1: $\rho=-0.84$, $p<0.0001$). Layer-specific differences in SOM compound group
663 abundances further indicated a progressive shift in the degree of organic matter transformation along the soil
664 profile that was consistent across polygon types. Organic topsoils were relatively enriched in lignins,
665 carbohydrates, and general and unknown compounds carbohydrates (Supplementary Fig. 4(b)), likely reflecting
666 inputs of little decomposed, labile plant detritus and root-derived substrates (Kuhry et al., 2020). In contrast,
667 mineral subsoils were characterized by the highest relative contributions of less bioavailable compound classes,
668 such as aromatics, phenols, and lipids. This likely reflects reduced inputs of fresh organic matter (Iversen et al.,
669 2015), together with restricted substrate exchange due to limited effective pore space pore water mobility in the
670 dense soil material, alongside mineral stabilization mechanisms (Dao et al., 2022; Prater et al., 2020).
671 Consequently, microbial communities in mineral subsoils rely more strongly on OM recycling, or on metabolizing
672 the accumulated, less bioavailable substrates (Weintraub and Schimel, 2003; Wild et al., 2016). Based on the
673 SOM ordination pattern and relative abundances of compound groups (Fig. 2(b); Supplementary Fig. 4(b)), the
674 permafrost SOM pool appeared structurally most similar to that of organic topsoils. This resemblance aligns well
675 with field observations of abundant structurally intact plant residues in the frozen material, and suggests that the
676 upper permafrost contains a substantial reservoir of relatively undecomposed organic matter that may become
677 microbially accessible upon thaw (Gentsch et al., 2018). Despite their relatively similar SOM profiles topsoils and
678 the upper permafrost layer differed most strongly in their microbial alpha and beta diversity patterns. By

679 comparison, C-rich cryoturbated material and its adjacent C-poor mineral soil hosted statistically indistinguishable
680 microbial communities (Figs. 3(b), 4(b)). Together, these patterns indicate that microbial community structure
681 along the soil profile is more strongly shaped by depth-related physicochemical constraints, such as temperature
682 or oxygen availability, than by SOM composition.

683 How microbiomes change along a permafrost soil profile has been of interest to a plethora of studies. These, in
684 line with our results (Supplementary Fig. 5, 9), reported a depth-dependent declines in microbial biomass (Jansson
685 and Taş, 2014; Liebner et al., 2008; Wild et al., 2016; Wilhelm et al., 2011), richness (Lipson et al., 2015), and
686 diversity (Frank-Fahle et al., 2014; Jansson and Taş, 2014; Liebner et al., 2008; Müller et al., 2018; Ping et al.,
687 1998; Taş et al., 2018). Also depth-dependent transitions in community structure and metabolic pathways are well
688 documented (Frank-Fahle et al., 2014; Mackelprang et al., 2011; Müller et al., 2018). In our dataset, a comparable
689 community shift was likely indicated by the steadily decreasing fraction of shared taxa between organic topsoils
690 and deeper layers (Supplementary Fig. 6(b), 10(b)). The permafrost layer exhibited the lowest microbial
691 abundance, richness and diversity of all investigated layers (Supplementary Fig. 5, 9), as the permafrost table
692 certainly marks a major physical and ecological boundary for microorganisms. In permafrost, subzero
693 temperatures, limited liquid water and oxygen availability, elevated salinity, and restricted exchange with the
694 active-layer microbiome (Doherty et al., 2020; Ernakovich et al., 2022), collectively select for specialized
695 communities (Jansson and Taş, 2014). For example, the permafrost layer harbored a notable fraction of ddPCR
696 corrected reads assigned to Cloacimonadota (68 %), Caldisericota (81 %), and Campylobacterota (93 %),
697 (Supplementary Table 6, Supplementary Fig.8), who comprise members that have been linked to anaerobic C
698 turnover, including fermentation and sulfur/nitrogen redox processes (Liu et al., 2025; Ratnikova et al., 2026; Sun
699 Qing-lei et al., 2023). Firmicutes were also abundant (54 %), consistent with their ability to persist in freeze-thaw
700 transition zones through dormancy and spore formation (Galperin, 2016). In contrast to the permafrost layer, the
701 organic layer emerged as pronounced microbial hotspot, especially for fungi (Supplementary Fig. 5, 9). Several
702 factors likely contributed to this pattern. First, most fungi are strongly confined to aerobic conditions (Zak and
703 Kling, 2006). Second, root biomass declines rapidly with depth in tundra soils (Iversen et al., 2015), leading to a
704 concomitant decrease in mycorrhizal associations (Gittel et al., 2014), as also observed in our dataset (8 % in
705 organic topsoils vs. 5 % in the permafrost layer; FunGuild analysis). Third, dominant decomposers of plant-
706 derived organic matter, such as Ascomycota and Basidiomycota (Wallenstein et al., 2007), may benefit from
707 cellulose- and lignin-rich substrate inputs into the topsoil layer (Boer et al., 2005).

708 Finally, the organic layer also emerged as a hotspot for hydrolytic enzyme activity (Fig. 5), likely due to its
709 exceptionally high microbial abundance per unit soil C, its comparatively diverse decomposer community
710 (Supplementary Fig. 5, 9), and high availability of little decomposed plant-derived substrates (Supplementary Fig.
711 4(b)). Notably, the permafrost layer exhibited relatively high enzyme activities despite harboring the lowest
712 microbial abundance and diversity (Fig. 5; Supplementary Fig. 12). This decoupling of microbial community
713 structure from enzyme potentials suggests that hydrolytic degradation capacity is largely governed by SOM
714 properties and less constrained by microbial abundance alone. At the same time, the substantial enzyme potential
715 observed in permafrost soils could also reflect the persistence of extracellular enzymes under chronically cold
716 conditions and/or a greater per-biomass investment in enzyme production required to access substrates in frozen
717 environments. Nonetheless, the pronounced latent enzymatic potential that we observed indicates that permafrost-
718 associated SOM may be rapidly mobilized following thaw.

719 *4.3 Potential links to carbon–climate feedbacks*

720 Widespread ice-wedge degradation has been documented across the Arctic (Abolt et al., 2020; Fraser et al., 2018;
721 Jorgenson et al., 2006, 2022; Kartoziia, 2019), largely in response to ongoing climate change. As permafrost
722 temperatures rise and disturbances such as thermokarst formation and flooding become more frequent, low-
723 centered polygons may increasingly transition into high-centered ones (Kartoziia, 2019; Kokelj et al., 2014;
724 Liljedahl et al., 2016; Nitzbon et al., 2019). Given that low-centered polygons in our study were characterized by
725 lower microbial abundance, reduced organic matter bioavailability, and diminished hydrolytic enzyme potential,
726 their conversion into high-centered polygons may accelerate soil carbon losses. Although drying tends to shift
727 carbon emissions from CH₄ toward the less potent CO₂ (Lara et al., 2015; Sachs et al., 2010), cumulative carbon
728 losses may still be higher (Lee et al., 2012a; Schädel et al., 2016).

729 Topsoils, here identified as hotspots of microbial abundance and hydrolytic degradation potential, are likely to be
730 most affected by future warming. Rising temperatures are expected to stimulate microbial activity (Hutchins et
731 al., 2019; Karhu et al., 2014; Schuur et al., 2015a), thereby increasing the potential for carbon release from these
732 carbon-rich horizons. However, warming also promotes active-layer deepening (Solomon et al., 2007; Westerveld
733 et al., 2023) and episodic thaw events, such as active-layer detachments, which expose previously frozen
734 substrates to microbial decomposition (Graham et al., 2012; Schmidt et al., 2011). Presuming that the upper
735 permafrost contained a substantial pool of relatively undecomposed organic matter and that permafrost microbes
736 exhibited considerable hydrolytic enzymatic potential, thaw progression could unlock significant additional
737 carbon losses.

738 Although accurate projections of tundra carbon balance require the integration of multiple ecosystem processes,
739 including vegetation dynamics (Myers-Smith et al., 2019; Phoenix and Treharne, 2022; Wolter et al., 2016),
740 rhizosphere priming effects (Friggens et al., 2025; Keuper et al., 2020; Wild et al., 2014, 2016), microbial
741 community assembly and coalescence (Ernakovich et al., 2022; Monteux et al., 2020), or couplings to other
742 biogeochemical cycles (Burke et al., 2022; Keuper et al., 2012; Treat et al., 2016), our findings highlight the
743 significance of spatial organization of lowland tundra landscapes for shaping soil organic matter pools, microbial
744 communities, and climate relevant biogeochemical dynamics.

745 **V. Conclusions**

746 Improving predictions of future water, energy, and carbon fluxes in Arctic lowland tundra requires explicit
747 treatment of its spatial heterogeneity. Here, we show how soil organic matter pools, microbial communities, and
748 hydrolytic enzyme potentials differ across ice wedge polygon types and soil layers, the two dominant axes of
749 edaphic variability in these ecosystems.

750 Strong polygon specific patterns persisted across all soil layers, and soil layer specific effects were consistent
751 across polygon types. This suggests that these two spatial dimensions largely act independently, with modest
752 interactions. Across both axes, patterns aligned with gradients in organic matter inputs and redox conditions,
753 which themselves arise from the dynamic interplay of microtopography, hydrology, and vegetation. These
754 environmental gradients, in turn, shape microbial communities and constrain characteristic biogeochemical
755 processes at both the polygon and soil layer scale.

756 Overall, our findings demonstrate that a limited set of spatial units captures a disproportionate share of edaphic,
757 microbial, and biogeochemical variability in Arctic lowland tundra soils. Explicitly accounting for polygon
758 morphology and major soil layers in ecosystem models, with low centered polygons and organic topsoils as
759 particularly informative and tractable units, therefore provides a practical framework for upscaling soil processes
760 in geomorphologically complex landscapes, and for improving climate-relevant biogeochemical projections.

761 **Data availability**

762 The data is accessible under: [10.5281/zenodo.18631833](https://zenodo.org/record/18631833).

763 **Competing interests**

764 The authors declare that they have no conflict of interest.

765 **Acknowledgements**

766 We gratefully acknowledge the dedicated logistical support provided by the team at AWI Potsdam during the
767 Yukon Coast expeditions in the summers of 2018 and 2019. We thank Hugues Lantuit for establishing the
768 foundation and framework that made this research possible, including funding, infrastructure, and permitting. We
769 are grateful to George Tanski for logistical assistance and field support during sample collection in 2018, Alberto
770 Canarini for significant assistance in developing the semi-automated pyrolysis-GC/MS fingerprinting workflow,
771 Leila Jensen for guidance on ddPCR measurements, and Petra Pjevac for coordinating the amplicon sequencing
772 process. We are especially thankful to Samuel McLeod, Frank Dillon, and Peter Archie for their invaluable
773 assistance, support, and insightful contributions in the field. We also appreciate the support provided by the Yukon
774 Territorial Government, Yukon Parks (Herschel Island – Qikiqtaruk Territorial Park), and the Aurora Research
775 Institute in Inuvik.

776 **Author contributions**

777 VM conducted the field and laboratory work, curated and analyzed the data, prepared visualizations, and wrote
778 the manuscript with input from co-authors. AR led the scientific conceptualization of the study, served as principal
779 supervisor of the research, and secured funding. AR and GH were responsible for project administration; GH also
780 provided scientific guidance and financial support for the expeditions. MF supported project administration and
781 fieldwork logistics, contributed expertise on the research area, and assisted with manuscript preparation.
782 Fieldwork was carried out by VM, JW, WAC, LD, RL, NS, AR, and GH. CR, JH, CUM, and MM assisted VM
783 with laboratory work and sample analyses. AR, VM, CR, and MM collaboratively developed the conceptual
784 framework for the pyrolysis–GC/MS fingerprinting methodology. CR also played a key role in data analysis
785 related to soil organic matter and microbial community composition. HS contributed to amplicon sequencing and
786 ddPCR assays and provided scientific input on microbial community analysis and manuscript preparation. BH
787 was responsible for sequencing methodology and raw data processing.

788 **Funding**

789 This work is part of the Project “Nunataryuk” and has received funding under the European Union’s Horizon 2020
790 Research and Innovation Program (grant agreement no. 773421).

791 **References**

- 792 Abarenkov, K., Zirk, A., Piirmann, T., Pöhönen, R., Ivanov, F., Nilsson, R. H., and Kõljalg, U.: UNITE general
 793 FASTA release for eukaryotes, 2. UNITE Community, <https://doi.org/10.15156/BIO/786371>, 2020.
- 794 Abolt, C. J., Young, M. H., Atchley, A. L., and Harp, D. R.: Microtopographic control on the ground thermal
 795 regime in ice wedge polygons, *The Cryosphere*, 12, 1957–1968, <https://doi.org/10.5194/tc-12-1957-2018>, 2018.
- 796 Abolt, C. J., Young, M. H., Atchley, A. L., Harp, D. R., and Coon, E. T.: Feedbacks Between Surface
 797 Deformation and Permafrost Degradation in Ice Wedge Polygons, Arctic Coastal Plain, Alaska, *Journal of*
 798 *Geophysical Research: Earth Surface*, 125, e2019JF005349, <https://doi.org/10.1029/2019JF005349>, 2020.
- 799 Aitchison, J.: The statistical analysis of geochemical compositions, *Journal of the International Association for*
 800 *Mathematical Geology*, 16, 531–564, <https://doi.org/10.1007/BF01029316>, 1984.
- 801 Alexander, E. B.: Bulk density equations for southern Alaska soils, *Canadian Journal of Soil Science*, 69, 177–
 802 180, <https://doi.org/10.4141/cjss89-017>, 1989.
- 803 Alteio, L. V., Séneca, J., Canarini, A., Angel, R., Jansa, J., Guseva, K., Kaiser, C., Richter, A., and Schmidt, H.:
 804 A critical perspective on interpreting amplicon sequencing data in soil ecological research, *Soil Biology and*
 805 *Biochemistry*, 160, <https://doi.org/10.1016/j.soilbio.2021.108357>, 2021.
- 806 Anderson, M.: Permutational Multivariate Analysis of Variance (PERMANOVA), 1–15,
 807 <https://doi.org/10.1002/9781118445112.stat07841>, 2017.
- 808 Apprill, A., McNally, S., Parsons, R., and Weber, L.: Minor revision to V4 region SSU rRNA 806R gene primer
 809 greatly increases detection of SAR11 bacterioplankton, *Aquatic Microbial Ecology*, 75, 129–137, 2015.
- 810 Arora, B., Wainwright, H. M., Dwivedi, D., Vaughn, L. J. S., Curtis, J. B., Torn, M. S., Dafflon, B., and
 811 Hubbard, S. S.: Evaluating temporal controls on greenhouse gas (GHG) fluxes in an Arctic tundra environment:
 812 An entropy-based approach, *Science of The Total Environment*, 649, 284–299,
 813 <https://doi.org/10.1016/j.scitotenv.2018.08.251>, 2019.
- 814 Baker, C. C. M., Barker, A. J., Douglas, T. A., Doherty, S. J., and Barbato, R. A.: Seasonal variation in near-
 815 surface seasonally thawed active layer and permafrost soil microbial communities, *Environmental Research*
 816 *Letters*, 18, <https://doi.org/10.1088/1748-9326/acc542>, 2023.
- 817 Baldrian, P., Voříšková, J., Dobiášová, P., Merhautová, V., Lisá, L., and Valášková, V.: Production of
 818 extracellular enzymes and degradation of biopolymers by saprotrophic microfungi from the upper layers of
 819 forest soil, *Plant and Soil*, 338, 111–125, 2010.
- 820 Barbier, B. A., Dziduch, I., Liebner, S., Ganzert, L., Lantuit, H., Pollard, W., and Wagner, D.: Methane-cycling
 821 communities in a permafrost-affected soil on Herschel Island, Western Canadian Arctic: Active layer profiling
 822 of *mcrA* and *pmoA* genes, *FEMS Microbiology Ecology*, 82, 287–302, <https://doi.org/10.1111/j.1574-6941.2012.01332.x>, 2012.
- 824 Barlow, J. T., Bogatyrev, S. R., and Ismagilov, R. F.: A quantitative sequencing framework for absolute
 825 abundance measurements of mucosal and luminal microbial communities, *Nat Commun*, 11, 2590,
 826 <https://doi.org/10.1038/s41467-020-16224-6>, 2020.
- 827 Bastida, F., Eldridge, D. J., García, C., Kenny Png, G., Bardgett, R. D., and Delgado-Baquerizo, M.: Soil
 828 microbial diversity–biomass relationships are driven by soil carbon content across global biomes, *The ISME*
 829 *Journal*, 15, 2081–2091, <https://doi.org/10.1038/s41396-021-00906-0>, 2021.
- 830 Bates, D., Mächler, M., Bolker, B., and Walker, S.: Fitting Linear Mixed-Effects Models Using lme4, *Journal of*
 831 *Statistical Software*, 67, 1–48, <https://doi.org/10.18637/jss.v067.i01>, 2015.
- 832 Bauer, A.: Influence of Soil Organic Matter on Bulk Density and Available Water Capacity of Soils, Citation
 833 Key: Bauer1974InfluenceOS, 1974.

- 834 Beck, H., Zimmermann, N., McVicar, T., Vergopolan, N., Berg, A., and Wood, E.: Present and future Köppen-
835 Geiger climate classification maps at 1-km resolution, *Scientific Data*, 5, 180214,
836 <https://doi.org/10.1038/sdata.2018.214>, 2018.
- 837 Bending, G. D. and Read, D. J.: Nitrogen mobilization from protein-polyphenol complex by ericoid and
838 ectomycorrhizal fungi, *Soil Biology & Biochemistry*, 28, 1603–1612, 1996.
- 839 Boer, W. de, Folman, L. B., Summerbell, R. C., and Boddy, L.: Living in a fungal world: impact of fungi on soil
840 bacterial niche development*, *FEMS Microbiology Reviews*, 29, 795–811,
841 <https://doi.org/10.1016/j.femsre.2004.11.005>, 2005.
- 842 Boike, J., Wille, C., and Abnizova, A.: Climatology and summer energy and water balance of polygonal tundra
843 in the Lena River Delta, Siberia, *Journal of Geophysical Research: Biogeosciences*, 113,
844 <https://doi.org/10.1029/2007JG000540>, 2008.
- 845 Bottos, E. M., Kennedy, D. W., Romero, E. B., Fansler, S. J., Brown, J. M., Bramer, L. M., Chu, R. K., Tfaily,
846 M. M., Jansson, J. K., and Stegen, J. C.: Dispersal limitation and thermodynamic constraints govern spatial
847 structure of permafrost microbial communities, *FEMS Microbiology Ecology*, 94, fiy110,
848 <https://doi.org/10.1093/femsec/fiy110>, 2018.
- 849 Brooks, G. R. and Lane, L. S.: A guide to the landscape of the Firth River Valley, Ivvavik National Park, 2011.
- 850 Brown, J.: Tundra Soils Formed over Ice Wedges, Northern Alaska, *Soil Science Society of America Journal*,
851 31, 686–691, <https://doi.org/10.2136/sssaj1967.03615995003100050022x>, 1967.
- 852 Brune, A., Frenzel, P., and Cypionka, H.: Life at the oxic–anoxic interface: microbial activities and adaptations,
853 *FEMS Microbiology Reviews*, 24, 691–710, <https://doi.org/10.1111/j.1574-6976.2000.tb00567.x>, 2000.
- 854 Burke, E., Chadburn, S., and Huntingford, C.: Thawing Permafrost as a Nitrogen Fertiliser: Implications for
855 Climate Feedbacks, *Nitrogen*, 3, <https://doi.org/10.3390/nitrogen3020023>, 2022.
- 856 Burns, R. G., DeForest, J. L., Marxsen, J., Sinsabaugh, R. L., Stromberger, M. E., Wallenstein, M. D.,
857 Weintraub, M. N., and Zoppini, A.: Soil enzymes in a changing environment: Current knowledge and future
858 directions, *Soil Biology and Biochemistry*, 58, 216–234, <https://doi.org/10.1016/j.soilbio.2012.11.009>, 2013.
- 859 Callahan, B. J., Sankaran, K., Fukuyama, J. A., McMurdie, P. J., and Holmes, S. P.: Bioconductor Workflow for
860 Microbiome Data Analysis: from raw reads to community analyses, *F1000Research*, 5,
861 <https://doi.org/10.12688/f1000research.8986.2>, 2016a.
- 862 Callahan, B. J., McMurdie, P. J., Rosen, M. J., Han, A. W., Johnson, A. J. A., and Holmes, S. P.: DADA2:
863 High-resolution sample inference from Illumina amplicon data, *Nature Methods*, 13, 581–583,
864 <https://doi.org/10.1038/nmeth.3869>, 2016b.
- 865 Canarini, A., Schmidt, H., Fuchslueger, L., Martin, V., Herbold, C. W., Zezula, D., Gündler, P., Hasibeder, R.,
866 Jecmenica, M., Bahn, M., and Richter, A.: Ecological memory of recurrent drought modifies soil processes via
867 changes in soil microbial community, *Nature Communications*, 12, 1–14, <https://doi.org/10.1038/s41467-021-25675-4>, 2021.
- 869 Chen, W., Tape, K. D., Euskirchen, E. S., Liang, S., Matos, A., Greenberg, J., and Fraterrigo, J. M.: Impacts of
870 Arctic Shrubs on Root Traits and Belowground Nutrient Cycles Across a Northern Alaskan Climate Gradient.,
871 *Frontiers in plant science*, 11, 588098, <https://doi.org/10.3389/fpls.2020.588098>, 2020.
- 872 Chu, H., Neufeld, J. D., Walker, V. K., and Grogan, P.: The Influence of Vegetation Type on the Dominant Soil
873 Bacteria, Archaea, and Fungi in a Low Arctic Tundra Landscape, *Soil Science Society of America Journal*, 75,
874 1756–1765, <https://doi.org/10.2136/sssaj2011.0057>, 2011.
- 875 Clymo, R. S. and Hayward, P. M.: *The Ecology of Sphagnum - Bryophyte Ecology*, edited by: Smith, A. J. E.,
876 Springer Netherlands, Dordrecht, 229–289, https://doi.org/10.1007/978-94-009-5891-3_8, 1982.

- 877 Couture, N. J. and Pollard, W. H.: A Model for Quantifying Ground-Ice Volume, Yukon Coast, Western Arctic
878 Canada, *Permafrost and Periglacial Processes*, 28, 534–542, <https://doi.org/10.1002/ppp.1952>, 2017.
- 879 D’Angelo, E. and Crutchfield, J.: Rapid, Sensitive, Microscale Determination of Phosphate in Water and Soil,
880 *Journal of Environment Quality*, 30, 2206, 2001.
- 881 Dao, T. T., Mikutta, R., Sauheitl, L., Gentsch, N., Shibistova, O., Wild, B., Schneckner, J., Bárta, J., Čapek, P.,
882 Gittel, A., Lashchinskiy, N., Urich, T., Šantrůčková, H., Richter, A., and Guggenberger, G.: Lignin Preservation
883 and Microbial Carbohydrate Metabolism in Permafrost Soils, *Journal of Geophysical Research: Biogeosciences*,
884 127, <https://doi.org/10.1029/2020JG006181>, 2022.
- 885 Doherty, S. J., Barbato, R. A., Grandy, A. S., Thomas, W. K., Monteux, S., Dorrepaal, E., Johansson, M., and
886 Ernakovich, J. G.: The Transition From Stochastic to Deterministic Bacterial Community Assembly During
887 Permafrost Thaw Succession, *Frontiers in Microbiology*, Volume 11-2020, 2020.
- 888 Doherty, S. J., Thurston, A. K., and Barbato, R. A.: Active layer and permafrost microbial community
889 coalescence increases soil activity and diversity in mixed communities compared to permafrost alone, *Frontiers*
890 *in Microbiology*, Volume 16-2025, 2025.
- 891 Donner, N., Minke, M., de Klerk, P., Sofronov, R., and Joosten, H.: Patterns in polygon mires in north-eastern
892 Yakutia, Siberia: the role of vegetation and water, *The Finnish Environment*, 38, 19–30, 2012.
- 893 Dungait, J. A. J., Hopkins, D. W., Gregory, A. S., and Whitmore, A. P.: Soil organic matter turnover is
894 governed by accessibility not recalcitrance, *Global Change Biology*, 18, 1781–1796,
895 <https://doi.org/10.1111/j.1365-2486.2012.02665.x>, 2012.
- 896 Ernakovich, J. G., Lynch, L. M., Brewer, P. E., Calderon, F. J., and Wallenstein, M. D.: Redox and temperature-
897 sensitive changes in microbial communities and soil chemistry dictate greenhouse gas loss from thawed
898 permafrost, *Biogeochemistry*, 134, 183–200, <https://doi.org/10.1007/s10533-017-0354-5>, 2017.
- 899 Ernakovich, J. G., Barbato, R. A., Rich, V. I., Schädel, C., Hewitt, R. E., Doherty, S. J., Whalen, E. D., Abbott,
900 B. W., Barta, J., Biasi, C., Chabot, C. L., Hultman, J., Knoblauch, C., Mackelprang, R., Onstott, T. C., Richter,
901 A., Vishnivetskaya, T. A., Waldrop, M. P., and Winkel, M.: Microbiome assembly in thawing permafrost and its
902 feedbacks to climate, 1–20, <https://doi.org/10.1111/gcb.16231>, 2022.
- 903 Fofana, A., Anderson, D., McCalley, C. K., Hodgkins, S., Wilson, R. M., Cronin, D., Raab, N., Torabi, M.,
904 Varner, R. K., Crill, P., Saleska, S. R., Chanton, J. P., Tfaily, M. M., and Rich, V. I.: Mapping substrate use
905 across a permafrost thaw gradient, *Soil Biology and Biochemistry*, 175, 108809,
906 <https://doi.org/10.1016/j.soilbio.2022.108809>, 2022.
- 907 Folhas, D., Couture, R.-M., Laurion, I., Vieira, G., and Canário, J.: Natural organic matter dynamics in
908 permafrost peatlands: Critical overview of recent findings and characterization tools, *TrAC Trends in Analytical*
909 *Chemistry*, 184, 118153, <https://doi.org/10.1016/j.trac.2025.118153>, 2025.
- 910 Fox, J. and Weisberg, S.: *An R Companion to Applied Regression*, Third Edition, Sage: Thousand Oaks, CA,
911 USA, 2019.
- 912 Frank-Fahle, B. A., Yergeau, É., Greer, C. W., Lantuit, H., and Wagner, D.: Microbial functional potential and
913 community composition in permafrost-affected soils of the NW Canadian Arctic, *PLoS ONE*, 9,
914 <https://doi.org/10.1371/journal.pone.0084761>, 2014.
- 915 Fraser, R. H., Kokelj, S. V., Lantz, T. C., McFarlane-Winchester, M., Olthof, I., and Lacelle, D.: Climate
916 Sensitivity of High Arctic Permafrost Terrain Demonstrated by Widespread Ice-Wedge Thermokarst on Banks
917 Island, *Remote Sensing*, 10, <https://doi.org/10.3390/rs10060954>, 2018.
- 918 Freeman, C., Ostle, N., and Kang, H.: An enzymic “latch” on a global carbon store, *Nature*, 409, 149–149,
919 <https://doi.org/10.1038/35051650>, 2001.

- 920 Freeman, C., Ostle, N. J., Fenner, N., and Kang, H.: A regulatory role for phenol oxidase during decomposition
921 in peatlands, *Soil Biology and Biochemistry*, 36, 1663–1667, <https://doi.org/10.1016/j.soilbio.2004.07.012>,
922 2004.
- 923 French, H. M.: *The Periglacial Environment*, Third Edition, John Wiley & Sons Ltd, West Sussex PO19 8SQ,
924 England, <https://doi.org/10.1002/9781118684931.ch8>, 2007.
- 925 Friggens, N. L., Hugelius, G., Kokelj, S. V., Murton, J. B., Phoenix, G. K., and Hartley, I. P.: Positive
926 rhizosphere priming accelerates carbon release from permafrost soils, *Nature Communications*, 16, 3576,
927 <https://doi.org/10.1038/s41467-025-58845-9>, 2025.
- 928 Fritz, M., Wetterich, S., Schirrmeister, L., Meyer, H., Lantuit, H., Preusser, F., and Pollard, W. H.: Eastern
929 Beringia and beyond: Late Wisconsinan and Holocene landscape dynamics along the Yukon Coastal Plain,
930 Canada, *Palaeogeography, Palaeoclimatology, Palaeoecology*, 319–320, 28–45,
931 <https://doi.org/10.1016/j.palaeo.2011.12.015>, 2012.
- 932 Fritz, M., Wolter, J., Rudaya, N., Palagushkina, O., Nazarova, L., Obu, J., Rethemeyer, J., Lantuit, H., and
933 Wetterich, S.: Holocene ice-wedge polygon development in northern Yukon permafrost peatlands (Canada),
934 *Quaternary Science Reviews*, 147, 279–297, <https://doi.org/10.1016/j.quascirev.2016.02.008>, 2016.
- 935 Galperin, M.: Genome Diversity of Spore-Forming Firmicutes, in: *The Bacterial Spore*, 1–18,
936 <https://doi.org/10.1128/9781555819323.ch1>, 2016.
- 937 Gentsch, N., Wild, B., Mikutta, R., Čapek, P., Diáková, K., Schrumpp, M., Turner, S., Minnich, C.,
938 Schaarschmidt, F., Shibistova, O., Schnecker, J., Urich, T., Gittel, A., Šantrůčková, H., Bárta, J., Lashchinskiy,
939 N., Fuß, R., Richter, A., and Guggenberger, G.: Temperature response of permafrost soil carbon is attenuated by
940 mineral protection, *Global Change Biology*, 24, 3401–3415, <https://doi.org/10.1111/gcb.14316>, 2018.
- 941 Gilichinsky, D., Rivkina, E., Shcherbakova, V., Laurinavichuis, K., and Tiedje, J.: Supercooled water brines
942 within permafrost-an unknown ecological niche for microorganisms: a model for astrobiology., *Astrobiology*,
943 3, 331–341, <https://doi.org/10.1089/153110703769016424>, 2003.
- 944 Gittel, A., Bárta, J., Kohoutová, I., Mikutta, R., Owens, S., Gilbert, J., Schnecker, J., Wild, B., Hannisdal, B.,
945 Maerz, J., Lashchinskiy, N., Čapek, P., Šantrůčková, H., Gentsch, N., Shibistova, O., Guggenberger, G.,
946 Richter, A., Torsvik, V. L., Schleper, C., and Urich, T.: Distinct microbial communities associated with buried
947 soils in the siberian tundra, *ISME Journal*, 8, 841–853, <https://doi.org/10.1038/ismej.2013.219>, 2014.
- 948 Gloor, G. B., Macklaim, J. M., Pawlowsky-Glahn, V., and Egozcue, J. J.: Microbiome Datasets Are
949 Compositional: And This Is Not Optional, *Front. Microbiol.*, 8, 2224, <https://doi.org/10.3389/fmicb.2017.02224>,
950 2017.
- 951 Graham, D. E., Wallenstein, M. D., Vishnivetskaya, T. A., Waldrop, M. P., Phelps, T. J., Pfiffner, S. M.,
952 Onstott, T. C., Whyte, L. G., Rivkina, E. M., Gilichinsky, D. A., Elias, D. A., Mackelprang, R., VerBerkmoes,
953 N. C., Hettich, R. L., Wagner, D., Wulschleger, S. D., and Jansson, J. K.: Microbes in thawing permafrost: the
954 unknown variable in the climate change equation, *The ISME Journal*, 6, 709–712,
955 <https://doi.org/10.1038/ismej.2011.163>, 2012.
- 956 Grosse, G., Harden, J., Turetsky, M., McGuire, A. D., Camill, P., Tarnocai, C., Frohking, S., Schuur, E. A. G.,
957 Jorgenson, T., Marchenko, S., Romanovsky, V., Wickland, K. P., French, N., Waldrop, M., Bourgeau-Chavez,
958 L., and Striegl, R. G.: Vulnerability of high-latitude soil organic carbon in North America to disturbance,
959 *Journal of Geophysical Research: Biogeosciences*, 116, <https://doi.org/10.1029/2010JG001507>, 2011.
- 960 Hatakka, A.: Biodegradation of Lignin, in: *Biopolymers Online*, <https://doi.org/10.1002/3527600035.bpol1005>,
961 2005.
- 962 Hubbard, S. S., Gangodagamage, C., Dafflon, B., Wainwright, H., Peterson, J., Gusmeroli, A., Ulrich, C., Wu,
963 Y., Wilson, C., Rowland, J., Tweedie, C., and Wulschleger, S. D.: Quantifying and relating land-surface and
964 subsurface variability in permafrost environments using LiDAR and surface geophysical datasets,
965 *Hydrogeology Journal*, 21, 149–169, <https://doi.org/10.1007/s10040-012-0939-y>, 2013.

- 966 Hugelius, G., Kuhry, P., Tarnocai, C., and Virtanen, T.: Soil organic carbon pools in a periglacial landscape: a
967 case study from the central Canadian Arctic, *Permafrost and Periglacial Processes*, 21, 16–29,
968 <https://doi.org/10.1002/ppp.677>, 2010.
- 969 Hultman, J., Waldrop, M. P., Mackelprang, R., David, M. M., McFarland, J., Blazewicz, S. J., Harden, J.,
970 Turetsky, M. R., McGuire, A. D., Shah, M. B., VerBerkmoes, N. C., Lee, L. H., Mavrommatis, K., and Jansson,
971 J. K.: Multi-omics of permafrost, active layer and thermokarst bog soil microbiomes, *Nature*, 521, 208–212,
972 <https://doi.org/10.1038/nature14238>, 2015.
- 973 Hutchins, D. A., Jansson, J. K., Remais, J. V., Rich, V. I., Singh, B. K., and Trivedi, P.: Climate change
974 microbiology — problems and perspectives, *Nature Reviews Microbiology*, 17, 391–396,
975 <https://doi.org/10.1038/s41579-019-0178-5>, 2019.
- 976 IPCC (Ed.): Polar Regions, in: *The Ocean and Cryosphere in a Changing Climate: Special Report of the*
977 *Intergovernmental Panel on Climate Change*, Cambridge University Press, Cambridge, 203–320,
978 <https://doi.org/10.1017/9781009157964.005>, 2022.
- 979 Irwin, A.: *Data Visualization - Making Maps*, 2021.
- 980 Iversen, C. M., Sloan, V. L., Sullivan, P. F., Euskirchen, E. S., McGuire, A. D., Norby, R. J., Walker, A. P.,
981 Warren, J. M., and Wulschleger, S. D.: The unseen iceberg: Plant roots in arctic tundra, *New Phytologist*, 205,
982 34–58, <https://doi.org/10.1111/nph.13003>, 2015.
- 983 Jackson, R. B., Canadell, J., Ehleringer, J. R., Mooney, H. A., Sala, O. E., and Schulze, E. D.: A global analysis
984 of root distributions for terrestrial biomes, *Oecologia*, 108, 389–411, <https://doi.org/10.1007/BF00333714>, 1996.
- 985 Jansson, J. and Taş, N.: The microbial ecology of permafrost, *Nature Reviews Microbiology*, 12, 414–425,
986 <https://doi.org/10.1038/nrmicro3262>, 2014.
- 987 Joabsson, A. and Christensen, T. R.: Methane emissions from wetlands and their relationship with vascular
988 plants: an Arctic example, *Global Change Biology*, 7, 919–932, <https://doi.org/10.1046/j.1354-1013.2001.00044.x>, 2001.
- 990 Johnston, E. R., Hatt, J. K., He, Z., Wu, L., Guo, X., Luo, Y., Schuur, E. A. G., Tiedje, J. M., Zhou, J., and
991 Konstantinidis, K. T.: Responses of tundra soil microbial communities to half a decade of experimental
992 warming at two critical depths, *Proc. Natl. Acad. Sci. U.S.A.*, 116, 15096–15105,
993 <https://doi.org/10.1073/pnas.1901307116>, 2019.
- 994 Jones, D. L.: Organic acids in the rhizosphere – a critical review, *Plant and Soil*, 205, 25–44,
995 <https://doi.org/10.1023/A:1004356007312>, 1998.
- 996 Jorgenson, M. T., Shur, Y. L., and Pullman, E. R.: Abrupt increase in permafrost degradation in Arctic Alaska,
997 *Geophysical Research Letters*, 33, <https://doi.org/10.1029/2005GL024960>, 2006.
- 998 Jorgenson, M. T., Kanevskiy, M. Z., Jorgenson, J. C., Liljedahl, A., Shur, Y., Epstein, H., Kent, K., Griffin, C.
999 G., Daanen, R., Boldenow, M., Orndahl, K., Witharana, C., and Jones, B. M.: Rapid transformation of tundra
1000 ecosystems from ice-wedge degradation, *Global and Planetary Change*, 216, 103921,
1001 <https://doi.org/10.1016/j.gloplacha.2022.103921>, 2022.
- 1002 Karhu, K., Auffret, M. D., Dungait, J. A. J., Hopkins, D. W., Prosser, J. I., Singh, B. K., Subke, J.-A., Wookey,
1003 P. A., Agren, G. I., Sebastià, M.-T., Gouriveau, F., Bergkvist, G., Meir, P., Nottingham, A. T., Salinas, N., and
1004 Hartley, I. P.: Temperature sensitivity of soil respiration rates enhanced by microbial community response.,
1005 *Nature*, 513, 81–84, <https://doi.org/10.1038/nature13604>, 2014.
- 1006 Kartoziia, A.: Assessment of the ice wedge polygon current state by means of UAV imagery analysis
1007 (Samoylov Island, the Lena Delta), *Remote Sensing*, 11, <https://doi.org/10.3390/rs11131627>, 2019.
- 1008 Keskitalo, K. H., Bröder, L., Shakil, S., Zolkos, S., Tank, S. E., van Dongen, B. E., Tesi, T., Haghypour, N.,
1009 Eglinton, T. I., Kokelj, S. V., and Vonk, J. E.: Downstream Evolution of Particulate Organic Matter
1010 Composition From Permafrost Thaw Slumps, *Frontiers in Earth Science*, Volume 9-2021, 2021.

- 1011 Keuper, F., Bodegom, P., Dorrepaal, E., Weedon, J., van Hal, J., Logtestijn, R., and Aerts, R.: A frozen feast:
1012 Thawing permafrost increases plant-available nitrogen in subarctic peatlands, *Global Change Biology*, 18,
1013 1998–2007, <https://doi.org/10.1111/j.1365-2486.2012.02663.x>, 2012.
- 1014 Keuper, F., Wild, B., Kummu, M., Beer, C., Blume-Werry, G., Fontaine, S., Gavazov, K., Gentsch, N.,
1015 Guggenberger, G., Hugelius, G., Jalava, M., Koven, C., Krab, E. J., Kuhry, P., Monteux, S., Richter, A.,
1016 Shahzad, T., Weedon, J. T., and Dorrepaal, E.: Carbon loss from northern circumpolar permafrost soils
1017 amplified by rhizosphere priming, *Nature Geoscience*, 13, 560–565, <https://doi.org/10.1038/s41561-020-0607-0>,
1018 2020.
- 1019 Knoblauch, C., Beer, C., Liebner, S., Grigoriev, M. N., and Pfeiffer, E. M.: Methane production as key to the
1020 greenhouse gas budget of thawing permafrost, *Nature Climate Change*, 8, 1–4, [https://doi.org/10.1038/s41558-](https://doi.org/10.1038/s41558-018-0095-z)
1021 018-0095-z, 2018.
- 1022 Kokelj, S. V., Lantz, T. C., Wolfe, S. A., Kanigan, J. C., Morse, P. D., Coutts, R., Molina-Giraldo, N., and Burn,
1023 C. R.: Distribution and activity of ice wedges across the forest-tundra transition, western Arctic Canada, *Journal*
1024 *of Geophysical Research: Earth Surface*, 119, 2032–2047, <https://doi.org/10.1002/2014JF003085>, 2014.
- 1025 Kostka, J., Weston, D., Glass, J., Lilleskov, E., Shaw, A., and Turetsky, M.: The Sphagnum microbiome: New
1026 insights from an ancient plant lineage, *The New phytologist*, 211, <https://doi.org/10.1111/nph.13993>, 2016.
- 1027 Krantz, W. B.: Self-organization manifest as patterned ground in recurrently frozen soils, *Earth-Science*
1028 *Reviews*, 29, 117–130, [https://doi.org/10.1016/0012-8252\(0\)90031-P](https://doi.org/10.1016/0012-8252(0)90031-P), 1990.
- 1029 Kuhry, Peter., Barta, Jiri., Blok, Daan., Elberling, Bo., Faucherre, Samuel., Hugelius, Gustaf., Jørgensen, C. J.,
1030 Richter, Andreas., Šantráčková, Hana., and Weiss, Niels.: Lability classification of soil organic matter in the
1031 northern permafrost region, *Biogeosciences*, 17, 361–379, <https://doi.org/10.5194/bg-17-361-2020>, 2020.
- 1032 Kuo, S.: Phosphorus. In *Methods of Soil Analysis, Part 3: Chemical Methods.*, Soil Science Society of America,
1033 869–919 pp., 1996.
- 1034 Kuznetsova, A., Brockhoff, P. B., and Christensen, R. H. B.: lmerTest Package: Tests in Linear Mixed Effects
1035 Models, *Journal of Statistical Software*, 82, 1–26, <https://doi.org/10.18637/jss.v082.i13>, 2017.
- 1036 Kwon, M. J., Jung, J. Y., Tripathi, B. M., Göckede, M., Lee, Y. K., and Kim, M.: Dynamics of microbial
1037 communities and CO₂ and CH₄ fluxes in the tundra ecosystems of the changing Arctic, *Journal of*
1038 *Microbiology*, 57, 325–336, <https://doi.org/10.1007/s12275-019-8661-2>, 2019.
- 1039 Langsrud, Ø.: ANOVA for unbalanced data: Use Type II instead of Type III sums of squares, *Statistics and*
1040 *computing*, 13, 163–167, 2003.
- 1041 Lara, M. J., McGuire, A. David., Euskirchen, E. S., Tweedie, C. E., Hinkel, K. M., Skurikhin, A. N.,
1042 Romanovsky, V. E., Grosse, Guido., Bolton, W. Robert., and Genet, Helene.: Polygonal tundra
1043 geomorphological change in response to warming alters future CO₂ and CH₄ flux on the Barrow Peninsula,
1044 *Global Change Biology*, 21, 1634–1651, <https://doi.org/10.1111/gcb.12757>, 2015.
- 1045 Lara, M. J., Nitze, I., Grosse, G., and McGuire, A. D.: Tundra landform and vegetation productivity trend maps
1046 for the Arctic Coastal Plain of northern Alaska, *Scientific Data*, 5, 180058,
1047 <https://doi.org/10.1038/sdata.2018.58>, 2018.
- 1048 Lee, H., Schuur, E. A. G., Inglett, K. S., Lavoie, M., and Chanton, J. P.: The rate of permafrost carbon release
1049 under aerobic and anaerobic conditions and its potential effects on climate, *Global Change Biology*, 18, 515–
1050 527, <https://doi.org/10.1111/j.1365-2486.2011.02519.x>, 2012a.
- 1051 Lee, S., Jang, I., Chae, N., Choi, T., and Kang, H.: Organic Layer Serves as a Hotspot of Microbial Activity and
1052 Abundance in Arctic Tundra Soils, *Microbial ecology*, 65, <https://doi.org/10.1007/s00248-012-0125-8>, 2012b.
- 1053 Lenth, R. V., Buerkner, P., Herve, M., Love, J., Miguez, F., Riebl, H., and Singmann, H.: Package
1054 “Emmeans”(Version R Package 1.7. 2): Estimated Marginal Means, Aka Least-Squares Means [Computer
1055 Software], 2022.

- 1056 Liebner, S., Harder, J., and Wagner, D.: Bacterial diversity and community structure in polygonal tundra soils
1057 from Samoylov Island, Lena Delta, Siberia, *International Microbiology*, 11, 195–202,
1058 <https://doi.org/10.2436/20.1501.01.60>, 2008.
- 1059 Liljedahl, A. K., Boike, J., Daanen, R. P., Fedorov, A. N., Frost, G. V., Grosse, G., Hinzman, L. D., Iijma, Y.,
1060 Jorgenson, J. C., Matveyeva, N., Necsoiu, M., Reynolds, M. K., Romanovsky, V. E., Schulla, J., Tape, K. D.,
1061 Walker, D. A., Wilson, C. J., Yabuki, H., and Zona, D.: Pan-Arctic ice-wedge degradation in warming
1062 permafrost and its influence on tundra hydrology, *Nature Geoscience*, 9, 312–318,
1063 <https://doi.org/10.1038/ngeo2674>, 2016.
- 1064 Lipson, D. A., Haggerty, J. M., Srinivas, A., Raab, T. K., Sathe, S., and Dinsdale, E. A.: Metagenomic Insights
1065 into Anaerobic Metabolism along an Arctic Peat Soil Profile, *PLoS ONE*, 8,
1066 <https://doi.org/10.1371/journal.pone.0064659>, 2013.
- 1067 Lipson, D. A., Raab, T. K., Parker, M., Kelley, S. T., Brislawn, C. J., and Jansson, J.: Changes in microbial
1068 communities along redox gradients in polygonized Arctic wet tundra soils, *Environmental Microbiology*
1069 *Reports*, 7, 649–657, <https://doi.org/10.1111/1758-2229.12301>, 2015.
- 1070 Liu, Y., Yu, M., Chen, X., Ran, L., and Zhang, X.-H.: Diversity, metabolic potential and global distribution of
1071 the anaerobic fermentative bacteria Phylum Candidatus Cloacimonadota, *Environmental Microbiome*, 20, 136,
1072 <https://doi.org/10.1186/s40793-025-00796-1>, 2025.
- 1073 Lynch, L., Margenot, A., Calderon, F., and Ernakovich, J.: Greater regulation of permafrost organic matter
1074 composition by enzymes and redox than temperature, *Soil Biology and Biochemistry*, 180, 108991,
1075 <https://doi.org/10.1016/j.soilbio.2023.108991>, 2023.
- 1076 Lynch, L. M., Machmuller, M. B., Cotrufo, M. F., Paul, E. A., and Wallenstein, M. D.: Tracking the fate of
1077 fresh carbon in the Arctic tundra: Will shrub expansion alter responses of soil organic matter to warming?, *Soil*
1078 *Biology and Biochemistry*, 120, 134–144, <https://doi.org/10.1016/j.soilbio.2018.02.002>, 2018.
- 1079 MacKay, J.: Thermally induced movements in ice-wedge polygons, Western Arctic Coast: A long-term study,
1080 *Géographie physique et Quaternaire*, 54, 41, <https://doi.org/10.7202/004846ar>, 2000.
- 1081 Mackelprang, R., Waldrop, M. P., Deangelis, K. M., David, M. M., Chavarria, K. L., Blazewicz, S. J., Rubin, E.
1082 M., and Jansson, J. K.: Metagenomic analysis of a permafrost microbial community reveals a rapid response to
1083 thaw, *Nature*, 480, 368–371, <https://doi.org/10.1038/nature10576>, 2011.
- 1084 Mackelprang, R., Saleska, S. R., Jacobsen, C. S., Jansson, J. K., and Taş, N.: Permafrost Meta-Omics and
1085 Climate Change, *Annual Review of Earth and Planetary Sciences*, 44, 439–462,
1086 <https://doi.org/10.1146/annurev-earth-060614-105126>, 2016.
- 1087 Madigan, M., Sattley, W., Aiyer, J., Stahl, D., and Buckley, D.: *Brock Biology of Microorganisms*, Global
1088 Edition, Pearson Deutschland, 1128 pp., 2021.
- 1089 Malard, L. A. and Pearce, D. A.: Microbial diversity and biogeography in Arctic soils, *Environmental*
1090 *Microbiology Reports*, 10, 611–625, <https://doi.org/10.1111/1758-2229.12680>, 2018.
- 1091 Malmer, N. and Holm, E.: Variation in the C/N-Quotient of Peat in Relation to Decomposition Rate and Age
1092 Determination with ²¹⁰Pb, *Oikos*, 43, 171–182, <https://doi.org/10.2307/3544766>, 1984.
- 1093 Martin, V., Schmidt, H., Canarini, A., Koranda, M., Hausmann, B., Müller, C. W., and Richter, A.: Soil cover
1094 shapes organic matter pools and microbial communities in soils of maritime Antarctica, *Geoderma*, 446,
1095 116894, <https://doi.org/10.1016/j.geoderma.2024.116894>, 2024.
- 1096 Martinez Arbizu, P.: pairwiseAdonis: Pairwise multilevel comparison using adonis., 2020.
- 1097 McGonigle, T. P. and Turner, W. G.: Grasslands and Croplands Have Different Microbial Biomass Carbon
1098 Levels per Unit of Soil Organic Carbon, *Agriculture*, 7, <https://doi.org/10.3390/agriculture7070057>, 2017.

- 1099 McMurdie, P. J. and Holmes, S.: phyloseq: An R Package for Reproducible Interactive Analysis and Graphics
1100 of Microbiome Census Data, *PLOS ONE*, 8, 1–11, <https://doi.org/10.1371/journal.pone.0061217>, 2013.
- 1101 Minayeva, T., Sirin, A., Kershaw, P., and Bragg, O.: Arctic Peatlands, in: *The Wetland Book: II: Distribution,*
1102 *Description, and Conservation*, edited by: Finlayson, C. M., Milton, G. R., Prentice, R. C., and Davidson, N. C.,
1103 Springer Netherlands, Dordrecht, 275–288, https://doi.org/10.1007/978-94-007-4001-3_109, 2018.
- 1104 Monteux, S., Keuper, F., Fontaine, S., Gavazov, K., Hallin, S., Juhanson, J., Krab, E. J., Revaillet, S.,
1105 Verbruggen, E., Walz, J., Weedon, J. T., and Dorrepaal, E.: Carbon and nitrogen cycling in Yedoma permafrost
1106 controlled by microbial functional limitations, *Nature Geoscience*, 13, 794–798, [https://doi.org/10.1038/s41561-](https://doi.org/10.1038/s41561-020-00662-4)
1107 [020-00662-4](https://doi.org/10.1038/s41561-020-00662-4), 2020.
- 1108 Moorhead, D., Lashermes, G., and Sinsabaugh, R.: A theoretical model of C- and N-acquiring exoenzyme
1109 activities, which balances microbial demands during decomposition, *Soil Biology and Biochemistry*, 53, 133–
1110 141, <https://doi.org/10.1016/j.soilbio.2012.05.011>, 2012.
- 1111 Müller, O., Bang-Andreasen, T., White, R. A., Elberling, B., Taş, N., Kneafsey, T., Jansson, J. K., and Øvreås,
1112 L.: Disentangling the complexity of permafrost soil by using high resolution profiling of microbial community
1113 composition, key functions and respiration rates, *Environmental Microbiology*, 20, 4328–4342,
1114 <https://doi.org/10.1111/1462-2920.14348>, 2018.
- 1115 Myers-Smith, I., Kerby, J., Phoenix, G., Bjerke, J., Epstein, H., Assmann, J., John, C., Andreu-Hayles, L.,
1116 Angers-Blodin, S., Beck, P., Berner, L., Bhatt, U., Bjorkman, A., Blok, D., Bryn, A., Christiansen, C.,
1117 Cornelissen, J., Cunliffe, A., Elmendorf, S., and Wipf, S.: Complexity revealed in the greening of the Arctic, ,
1118 <https://doi.org/10.32942/osf.io/mzyjk>, 2019.
- 1119 Nitzbon, J., Langer, M., Westermann, S., Martin, L., Aas, K. S., and Boike, J.: Pathways of ice-wedge
1120 degradation in polygonal tundra under different hydrological conditions, *The Cryosphere*, 13, 1089–1123,
1121 <https://doi.org/10.5194/tc-13-1089-2019>, 2019.
- 1122 Oksanen, J., Blanchet, F. G., Friendly, M., Kindt, R., Legendre, P., McGlenn, D., Minchin, P. R., O'Hara, R. B.,
1123 Simpson, G. L., Solymos, P., Stevens, M. H. H., Szoecs, E., Wagner, H., 2020. *vegan: Community Ecology*
1124 *Package*. R package version 2.5-7. <https://CRAN.R-project.org/package=vegan>.
- 1125 Parada, A. E., Needham, D. M., and Fuhrman, J. A.: Every base matters: assessing small subunit rRNA primers
1126 for marine microbiomes with mock communities, time series and global field samples, *Environmental*
1127 *Microbiology*, 18, 1403–1414, <https://doi.org/10.1111/1462-2920.13023>, 2016.
- 1128 Phoenix, G. K. and Treharne, R.: Arctic greening and browning: Challenges and a cascade of complexities,
1129 *Global Change Biology*, 28, 3481–3483, <https://doi.org/10.1111/gcb.16118>, 2022.
- 1130 Ping, C. L., Bockheim, J. G., Kimble, J. M., Michaelson, G. J., and Walker, D. A.: Characteristics of cryogenic
1131 soils along a latitudinal transect in arctic Alaska, *Journal of Geophysical Research: Atmospheres*, 103, 28917–
1132 28928, <https://doi.org/10.1029/98JD02024>, 1998.
- 1133 Ping, C. L., Michaelson, G. J., Kimble, J. M., Romanovsky, V. E., Shur, Y. L., Swanson, D. K., and Walker, D.
1134 A.: Cryogenesis and soil formation along a bioclimate gradient in Arctic North America, *Journal of Geophysical*
1135 *Research: Biogeosciences*, 113, <https://doi.org/10.1029/2008JG000744>, 2008.
- 1136 Ping, C. L., Jastrow, J. D., Jorgenson, M. T., Michaelson, G. J., and Shur, Y. L.: Permafrost soils and carbon
1137 cycling, *SOIL*, 1, 147–171, <https://doi.org/10.5194/soil-1-147-2015>, 2015.
- 1138 Pjevac, P., Hausmann, B., Schwarz, J., Kohl, G., Herbold, C. W., Loy, A., and Berry, D.: An Economical and
1139 Flexible Dual Barcoding, Two-Step PCR Approach for Highly Multiplexed Amplicon Sequencing, *Frontiers in*
1140 *Microbiology*, 12, <https://doi.org/10.3389/fmicb.2021.669776>, 2021.
- 1141 Pölme, S., Abarenkov, K., Henrik Nilsson, R., Lindahl, B. D., Clemmensen, K. E., Kauserud, H., Nguyen, N.,
1142 Kjøller, R., Bates, S. T., Baldrian, P., Frøslev, T. G., Adojaan, K., Vizzini, A., Suija, A., Pfister, D., Baral, H.
1143 O., Järv, H., Madrid, H., Nordén, J., Liu, J. K., Pawlowska, J., Pöldmaa, K., Pärtel, K., Runnel, K., Hansen, K.,

- 1144 Larsson, K. H., Hyde, K. D., Sandoval-Denis, M., Smith, M. E., Toome-Heller, M., Wijayawardene, N. N.,
 1145 Menolli, N., Reynolds, N. K., Drenkhan, R., Maharachchikumbura, S. S. N., Gibertoni, T. B., Læssøe, T.,
 1146 Davis, W., Tokarev, Y., Corrales, A., Soares, A. M., Agan, A., Machado, A. R., Argüelles-Moyao, A.,
 1147 Detheridge, A., de Meiras-Otoni, A., Verbeken, A., Dutta, A. K., Cui, B. K., Pradeep, C. K., Marin, C.,
 1148 Stanton, D., Gohar, D., Wanasinghe, D. N., Otsing, E., Aslani, F., Griffith, G. W., Lumbsch, T. H., Grossart, H.
 1149 P., Masigol, H., Timling, I., Hiiesalu, I., Oja, J., Kupagme, J. Y., Geml, J., Alvarez-Manjarrez, J., Ilves, K., Loit,
 1150 K., Adamson, K., Nara, K., Küngas, K., Rojas-Jimenez, K., Biteniaks, K., Irinyi, L., Nagy, L. L., Soonvald, L.,
 1151 Zhou, L. W., Wagner, L., Aime, M. C., Öpik, M., Mujica, M. I., Metsoja, M., Ryberg, M., Vasar, M., Murata,
 1152 M., Nelsen, M. P., Cleary, M., Samarakoon, M. C., Doilom, M., Bahram, M., Hagh-Doust, N., Dulya, O.,
 1153 Johnston, P., Kohout, P., Chen, Q., Tian, Q., Nandi, R., Amiri, R., Perera, R. H., et al.: FungalTraits: a user-
 1154 friendly traits database of fungi and fungus-like stramenopiles, *Fungal Diversity*, 105,
 1155 <https://doi.org/10.1007/s13225-020-00466-2>, 2020.
- 1156 Prater, I., Zubrzycki, S., Buegger, F., Zoor-Füllgraff, L. C., Angst, G., Dannenmann, M., and Mueller, C. W.:
 1157 From fibrous plant residues to mineral-associated organic carbon -- the fate of organic matter in Arctic
 1158 permafrost soils, *Biogeosciences*, 17, 3367–3383, <https://doi.org/10.5194/bg-17-3367-2020>, 2020.
- 1159 Pruesse, E., Peplies, J., and Glöckner, F. O.: SINA: Accurate high-throughput multiple sequence alignment of
 1160 ribosomal RNA genes, *Bioinformatics*, 28, 1823–1829, <https://doi.org/10.1093/bioinformatics/bts252>, 2012.
- 1161 Quast, C., Pruesse, E., Yilmaz, P., Gerken, J., Schweer, T., Yarza, P., Peplies, J., and Glöckner, F. O.: The
 1162 SILVA ribosomal RNA gene database project: Improved data processing and web-based tools, *Nucleic Acids*
 1163 *Research*, 41, 590–596, <https://doi.org/10.1093/nar/gks1219>, 2013.
- 1164 Rampton, V. N.: Quaternary Geology Yukon Coastal Plain, Yukon Territory-Northwest Territory, ,
 1165 <https://doi.org/10.4095/111348>, 1982.
- 1166 Ratnikova, N. M., Merkel, A. Y., Novikov, A. A., and Slobodkin, A. I.: Isolation and characterization of
 1167 anaerobic thermophilic bacterium *Caldisericum insulae* sp.nov., the second cultivated representative of the
 1168 phylum *Caldisericota*, *Extremophiles*, 30, 7, <https://doi.org/10.1007/s00792-026-01418-5>, 2026.
- 1169 Read, D. J. and Perez-Moreno, J.: Mycorrhizas and nutrient cycling in ecosystems – a journey towards
 1170 relevance?, *New Phytologist*, 157, 475–492, <https://doi.org/10.1046/j.1469-8137.2003.00704.x>, 2003.
- 1171 Roy Chowdhury, T., Berns, E. C., Moon, J.-W., Gu, B., Liang, L., Wullschleger, S. D., and Graham, D. E.:
 1172 Temporal, Spatial, and Temperature Controls on Organic Carbon Mineralization and Methanogenesis in Arctic
 1173 High-Centered Polygon Soils, *Frontiers in Microbiology*, 11, <https://doi.org/10.3389/fmicb.2020.616518>, 2021.
- 1174 Sachs, T., Giebels, M., Boike, J., and Kutzbach, L.: Environmental controls on CH₄ emission from polygonal
 1175 tundra on the microsite scale in the Lena river delta, Siberia, *Global Change Biology*, 16, 3096–3110,
 1176 <https://doi.org/10.1111/j.1365-2486.2010.02232.x>, 2010.
- 1177 Schädel, C., Luo, Y., David Evans, R., Fei, S., and Schaeffer, S. M.: Separating soil CO₂ efflux into C-pool-
 1178 specific decay rates via inverse analysis of soil incubation data., *Oecologia*, 171, 721–732,
 1179 <https://doi.org/10.1007/s00442-012-2577-4>, 2013.
- 1180 Schädel, C., Schuur, E. A. G., Bracho, R., Elberling, B., Knoblauch, C., Lee, H., Luo, Y., Shaver, G. R., and
 1181 Turetsky, M. R.: Circumpolar assessment of permafrost C quality and its vulnerability over time using long-
 1182 term incubation data., *Global change biology*, 20, 641–652, <https://doi.org/10.1111/gcb.12417>, 2014.
- 1183 Schädel, C., Bader, M. K., Schuur, E. A. G., Biasi, C., Bracho, R., Čapek, P., Baets, S. D., Diáková, K.,
 1184 Ernakovich, J., Estop-aragones, C., Graham, D. E., Hartley, I. P., Iversen, C. M., Kane, E., Knoblauch, C.,
 1185 Lupascu, M., Martikainen, P. J., Natali, S. M., Norby, R. J., Donnell, J. A. O., Chowdhury, T. R., Šantrůčková,
 1186 H., Shaver, G., Sloan, V. L., Treat, C. C., Turetsky, M. R., Waldrop, M. P., and Wickland, K. P.: Potential
 1187 carbon emissions dominated by carbon dioxide from thawed permafrost soils, 6,
 1188 <https://doi.org/10.1038/NCLIMATE3054>, 2016.

- 1189 Schoeneberger, P. J., Wysocki, D. A., Benham, E. C., and Soil Survey Staff: Field Book for Describing and
 1190 Sampling Soils, Version 3.0, Natural Resources Conservation Service, National Soil Survey Center, Lincoln,
 1191 NE, ISBN: 9780160915420, 2012.
- 1192 Schmidt, M. W. I., Torn, M. S., Abiven, S., Dittmar, T., Guggenberger, G., Janssens, I. a., Kleber, M., Kögel-
 1193 Knabner, I., Lehmann, J., Manning, D. a. C., Nannipieri, P., Rasse, D. P., Weiner, S., and Trumbore, S. E.:
 1194 Persistence of soil organic matter as an ecosystem property, *Nature*, 478, 49–56,
 1195 <https://doi.org/10.1038/nature10386>, 2011.
- 1196 Schneckner, J., Wild, B., Takriti, M., Eloy Alves, R. J., Gentsch, N., Gittel, A., Hofer, A., Klaus, K., Knoltsch,
 1197 A., Lashchinskiy, N., Mikutta, R., and Richter, A.: Microbial community composition shapes enzyme patterns
 1198 in topsoil and subsoil horizons along a latitudinal transect in Western Siberia, *Soil Biology and Biochemistry*,
 1199 83, 106–115, <https://doi.org/10.1016/j.soilbio.2015.01.016>, 2015.
- 1200 Schneider, T., Keiblinger, K. M., Schmid, E., Sterflinger-Gleixner, K., Ellersdorfer, G., Roschitzki, B., Richter,
 1201 A., Eberl, L., Zechmeister-Boltenstern, S., and Riedel, K.: Who is who in litter decomposition? Metaproteomics
 1202 reveals major microbial players and their biogeochemical functions, *The ISME Journal*, 6, 1749–1762,
 1203 <https://doi.org/10.1038/ismej.2012.11>, 2012.
- 1204 Schuur, E., McGuire, A., Schädel, C., Grosse, G., Harden, J., Hayes, D. J., Hugelius, G., Koven, C., Kuhry, P.,
 1205 Lawrence, D., Natali, S., Olefeldt, D., Romanovsky, V., Schaefer, K., Turetsky, M., Treat, C., and Vonk, J.:
 1206 Climate change and the permafrost carbon feedback, *Nature*, 520, <https://doi.org/10.1038/nature14338>, 2015a.
- 1207 Schuur, E. A. G., Bockheim, J., Canadell, J. G., Euskirchen, E., Field, C. B., Goryachkin, S. V., Hagemann, S.,
 1208 Kuhry, P., Lafleur, P. M., Lee, H., Mazhitova, G., Nelson, F. E., Rinke, A., Romanovsky, V. E., Shiklomanov,
 1209 N., Tarnocai, C., Venevsky, S., Vogel, J. G., and Zimov, S. A.: Vulnerability of Permafrost Carbon to Climate
 1210 Change: Implications for the Global Carbon Cycle, *BioScience*, 58, 701–714, <https://doi.org/10.1641/B580807>,
 1211 2008.
- 1212 Schuur, E. A. G., McGuire, A. D., Schädel, C., Grosse, G., Harden, J. W., Hayes, D. J., Hugelius, G., Koven, C.
 1213 D., Kuhry, P., Lawrence, D. M., Natali, S. M., Olefeldt, D., Romanovsky, V. E., Schaefer, K., Turetsky, M. R.,
 1214 Treat, C. C., and Vonk, J. E.: Climate change and the permafrost carbon feedback, *Nature*, 520, 171–179,
 1215 <https://doi.org/10.1038/nature14338>, 2015b.
- 1216 Shaver, G. R., Chapin, F. S., and Billings, W. D.: Ecotypic Differentiation in *Carex Aquatilis* on Ice-Wedge
 1217 Polygons in the Alaskan Coastal Tundra, *Journal of Ecology*, 67, 1025–1045, <https://doi.org/10.2307/2259226>,
 1218 1979.
- 1219 Shur, Y., Hinkel, K. M., and Nelson, F. E.: The transient layer: implications for geocryology and climate-change
 1220 science, *Permafrost and Periglacial Processes*, 16, 5–17, <https://doi.org/10.1002/ppp.518>, 2005.
- 1221 Siewert, M. B., Lantuit, H., Richter, A., and Hugelius, G.: Permafrost causes unique fine-scale spatial variability
 1222 across tundra soils, *Global Biogeochemical Cycles*, 1–19, <https://doi.org/10.1029/2020gb006659>, 2021.
- 1223 Smith, D. P. and Peay, K. G.: Sequence depth, not PCR replication, improves ecological inference from next
 1224 generation DNA sequencing., *PloS one*, 9, e90234, <https://doi.org/10.1371/journal.pone.0090234>, 2014.
- 1225 Solomon, S., Qin, D., Manning, M., Chen, Z., Marquis, M., Averyt, K. B., Tignor, M., and Miller, H. L.:
 1226 *Climate Change 2007: The Physical Science Basis. Contribution of Working Group I to the Fourth Assessment*
 1227 *Report of the Intergovernmental Panel on Climate Change. Changes in the active layer.*, Cambridge University
 1228 Press, 2007.
- 1229 Speetjens, N. J., Tanski, G., Martin, V., Wagner, J., Richter, A., Hugelius, G., Boucher, C., Lodi, R.,
 1230 Knoblauch, C., Koch, B. P., Wünsch, U., Lantuit, H., and Vonk, J. E.: Dissolved organic matter characterization
 1231 in soils and streams in a small coastal low-Arctic catchment, *Biogeosciences*, 19, 3073–3097,
 1232 <https://doi.org/10.5194/bg-19-3073-2022>, 2022.

- 1233 Sturtevant, C. S. and Oechel, W. C.: Spatial variation in landscape-level CO₂ and CH₄ fluxes from arctic
1234 coastal tundra: influence from vegetation, wetness, and the thaw lake cycle, *Global Change Biology*, 19, 2853–
1235 2866, <https://doi.org/10.1111/gcb.12247>, 2013.
- 1236 Sun Qing-lei, Xu Ke, Cao Lei, Du Zengfeng, Wang Minxiao, and Sun Li: Nitrogen and sulfur cycling driven by
1237 Campylobacterota in the sediment–water interface of deep-sea cold seep: a case in the South China Sea, *mBio*,
1238 14, e00117-23, <https://doi.org/10.1128/mbio.00117-23>, 2023.
- 1239 Taş, N., Prestat, E., Wang, S., Wu, Y., Ulrich, C., Kneafsey, T., Tringe, S. G., Torn, M. S., Hubbard, S. S., and
1240 Jansson, J. K.: Landscape topography structures the soil microbiome in arctic polygonal tundra, *Nature*
1241 *Communications*, 9, <https://doi.org/10.1038/s41467-018-03089-z>, 2018.
- 1242 Treat, C. C., Wollheim, W. M., Varner, R. K., Grandy, A. S., Talbot, J., and Froelking, S.: Temperature and peat
1243 type control CO₂ and CH₄ production in Alaskan permafrost peats, *Global Change Biology*, 20, 2674–2686,
1244 <https://doi.org/10.1111/gcb.12572>, 2014.
- 1245 Treat, C. C., Wollheim, W. M., Varner, R. K., and Bowden, W. B.: Longer thaw seasons increase nitrogen
1246 availability for leaching during fall in tundra soils, *Environmental Research Letters*, 11,
1247 <https://doi.org/10.1088/1748-9326/11/6/064013>, 2016.
- 1248 Turetsky, M. R.: The Role of Bryophytes in Carbon and Nitrogen Cycling, *The Bryologist*, 106, 395–409, 2003.
- 1249 Tveit, A., Schwacke, R., Svenning, M. M., and Urich, T.: Organic carbon transformations in high-Arctic peat
1250 soils: Key functions and microorganisms, *ISME Journal*, 7, 299–311, <https://doi.org/10.1038/ismej.2012.99>,
1251 2013.
- 1252 Vandeputte, D., Kathagen, G., D’hoë, K., Vieira-Silva, S., Valles-Colomer, M., Sabino, J., Wang, J., Tito, R. Y.,
1253 De Commer, L., Darzi, Y., Vermeire, S., Falony, G., and Raes, J.: Quantitative microbiome profiling links gut
1254 community variation to microbial load, *Nature*, 551, 507–511, <https://doi.org/10.1038/nature24460>, 2017.
- 1255 Vaughn, L. J. S. and Torn, M. S.: Radiocarbon measurements of ecosystem respiration and soil pore-space CO₂
1256 in Utqiagvik (Barrow), Alaska, *Earth System Science Data*, 10, 1943–1957, <https://doi.org/10.5194/essd-10-1943-2018>, 2018.
- 1258 Verret, M., Naeher, S., Lacelle, D., Ginnane, C., Dickinson, W., Norton, K., Turnbull, J., and Levy, R.:
1259 Preservation and degradation of ancient organic matter in mid-Miocene Antarctic permafrost, *Biogeosciences*,
1260 22, 5771–5786, <https://doi.org/10.5194/bg-22-5771-2025>, 2025.
- 1261 Vives-Peris, V., de Ollas, C., Gómez-Cadenas, A., and Pérez-Clemente, R. M.: Root exudates: from plant to
1262 rhizosphere and beyond, *Plant Cell Reports*, 39, 3–17, <https://doi.org/10.1007/s00299-019-02447-5>, 2020.
- 1263 Voigt, C., Lind, S. E., Lamprecht, R. E., Biasi, C., Martikainen, P. J., Marushchak, M. E., Novakovskiy, A., and
1264 Aurela, M.: Warming of subarctic tundra increases emissions of all three important greenhouse gases - carbon
1265 dioxide, methane, and nitrous oxide, *Global Change Biology*, 23, 3121–3138,
1266 <https://doi.org/10.1111/gcb.13563>, 2016.
- 1267 Wagner, J., Martin, V., Speetjens, N. J., A’Campo, W., Durstewitz, L., Lodi, R., Fritz, M., Tanski, G., Vonk, J.
1268 E., Richter, A., Bartsch, A., Lantuit, H., and Hugelius, G.: High resolution mapping shows differences in soil
1269 carbon and nitrogen stocks in areas of varying landscape history in Canadian lowland tundra, *Geoderma*, 438,
1270 116652, <https://doi.org/10.1016/j.geoderma.2023.116652>, 2023.
- 1271 Wainwright, Haruko., Dafflon, Baptiste., Smith, Lydia., Hahn, Melanie., Curtis, John., Wu, Yuxin., Ulrich,
1272 Craig., Peterson, John., Torn, Margaret., and Hubbard, Susan.: Identifying multiscale zonation and assessing the
1273 relative importance of polygon geomorphology on carbon fluxes in an Arctic tundra ecosystem, *Journal of*
1274 *Geophysical Research: Biogeosciences*, 788–808, <https://doi.org/10.1002/2014JG002799>.Received, 2015.
- 1275 Waldrop, M. P., Chabot, C. L., Liebner, S., Holm, S., Snyder, M. W., Dillon, M., Dudgeon, S. R., Douglas, T.
1276 A., Leewis, M.-C., Walter Anthony, K. M., McFarland, J. W., Arp, C. D., Bondurant, A. C., Taş, N., and
1277 Mackelprang, R.: Permafrost microbial communities and functional genes are structured by latitudinal and soil
1278 geochemical gradients, *The ISME Journal*, 17, 1224–1235, <https://doi.org/10.1038/s41396-023-01429-6>, 2023.

- 1279 Waldrop, M. P., Ernakovich, J. G., Vishnivetskaya, T. A., Schaefer, S. R., Mackelprang, R., Barta, J., O'Brien,
1280 J. M., Winkel, M., Barbato, R. A., Heffernan, L., Leewis, M. C., Hewitt, R. E., Hultman, J., Sun, Y., Biasi, C.,
1281 Bradley, J. A., Liebner, S., Ricketts, M. P., Muscarella, M. E., Schütte, U., Abuah, F., Whalen, E., Timling, I.,
1282 Voigt, C., Taş, N., Lloyd, K. G., Siljanen, H. M. P., Rivkina, E. M., Voříšková, J., Tao, J., Liang, R., Li, Z.,
1283 Lennon, J. T., and Onstott, T. C.: Microbial Ecology of Permafrost Soils: Populations, Processes, and
1284 Perspectives, Permafrost and Periglacial Processes, 1–14, <https://doi.org/10.1002/ppp.2264>, 2025.
- 1285 Walker, D. A., Raynolds, M. K., Daniëls, F. J. A., Einarsson, E., Elvebakk, A., Gould, W. A., Katenin, A. E.,
1286 Kholod, S. S., Markon, C. J., Melnikov, E. S., Moskalenko, N. G., Talbot, S. S., Yurtsev, B. A. (†), and Team,
1287 T. other members of the C.: The Circumpolar Arctic vegetation map, *Journal of Vegetation Science*, 16, 267–
1288 282, <https://doi.org/10.1111/j.1654-1103.2005.tb02365.x>, 2005.
- 1289 Wallenstein, M. D., McMahon, S., and Schimel, J.: Bacterial and fungal community structure in Arctic tundra
1290 tussock and shrub soils, *FEMS microbiology ecology*, 59, 428–435, [https://doi.org/10.1111/j.1574-](https://doi.org/10.1111/j.1574-6941.2006.00260.x)
1291 [6941.2006.00260.x](https://doi.org/10.1111/j.1574-6941.2006.00260.x), 2007.
- 1292 Walvoord, M. A. and Kurylyk, B. L.: Hydrologic Impacts of Thawing Permafrost—A Review, *Vadose Zone*
1293 *Journal*, 15, [vzj2016.01.0010](https://doi.org/10.2136/vzj2016.01.0010), <https://doi.org/10.2136/vzj2016.01.0010>, 2016.
- 1294 Washburn, A. L.: Classification of patterned ground and review of suggested origins, *GSA Bulletin*, 67, 823–
1295 866, [https://doi.org/10.1130/0016-7606\(1956\)67%255B823:COPGAR%255D2.0.CO;2](https://doi.org/10.1130/0016-7606(1956)67%255B823:COPGAR%255D2.0.CO;2), 1956.
- 1296 Washburn, A. L.: Periglacial processes and environments, St. Martin's Press, New York, 1973.
- 1297 Weintraub, M. N. and Schimel, J. P.: Interactions between carbon and nitrogen mineralization and soil organic
1298 matter chemistry in arctic tundra soils, *Ecosystems*, 6, 129–143, <https://doi.org/10.1007/s10021-002-0124-6>,
1299 2003.
- 1300 Weiss, N., Blok, D., Elberling, B., Hugelius, G., Jørgensen, C. J., Siewert, M. B., and Kuhry, P.: Thermokarst
1301 dynamics and soil organic matter characteristics controlling initial carbon release from permafrost soils in the
1302 Siberian Yedoma region, *Sedimentary Geology*, 340, 38–48, <https://doi.org/10.1016/j.sedgeo.2015.12.004>,
1303 2016.
- 1304 Westerveld, L., Kurvits, T., Schoolmeester, T., Eckhoff, T., Overduin, P., Fritz, M., Alftan, B., Sinisalo, A.,
1305 and Mulelid, O.: Arctic Permafrost Atlas, <https://doi.org/10.61523/KPJI4549>, 2023.
- 1306 White, Bruns, T., Lee, S., and Taylor, J.: White, T. J., T. D. Bruns, S. B. Lee, and J. W. Taylor. Amplification
1307 and direct sequencing of fungal ribosomal RNA Genes for phylogenetics, 315–322, 1990.
- 1308 Wickham, H.: *ggplot2: Elegant Graphics for Data Analysis*, Springer International Publishing, 2016.
- 1309 Wild, B., Schneckner, J., Alves, R. J. E., Barsukov, P., Bárta, J., Čapek, P., Gentsch, N., Gittel, A.,
1310 Guggenberger, G., Lashchinskiy, N., Mikutta, R., Rusalimova, O., Šantrůčková, H., Shibistova, O., Urich, T.,
1311 Watzka, M., Zrazhevskaya, G., and Richter, A.: Input of easily available organic C and N stimulates microbial
1312 decomposition of soil organic matter in arctic permafrost soil, *Soil Biology and Biochemistry*, 75, 143–151,
1313 <https://doi.org/10.1016/j.soilbio.2014.04.014>, 2014.
- 1314 Wild, B., Gentsch, N., Capek, P., Diáková, K., Alves, R. J. E., Bárta, J., Gittel, A., Hugelius, G., Knoltsch, A.,
1315 Kuhry, P., Lashchinskiy, N., Mikutta, R., Palmtag, J., Schleper, C., Schneckner, J., Shibistova, O., Takriti, M.,
1316 Torsvik, V. L., Urich, T., Watzka, M., Šantrůčková, H., Guggenberger, G., and Richter, A.: Plant-derived
1317 compounds stimulate the decomposition of organic matter in arctic permafrost soils, *Scientific Reports*, 6, 1–11,
1318 <https://doi.org/10.1038/srep25607>, 2016.
- 1319 Wilhelm, R. C., Niederberger, T. D., Greer, C., and Whyte, L. G.: Microbial diversity of active layer and
1320 permafrost in an acidic wetland from the Canadian high arctic, *Canadian Journal of Microbiology*, 57, 303–315,
1321 <https://doi.org/10.1139/w11-004>, 2011.
- 1322 Wilson, R. M., Hough, M. A., Verbeke, B. A., Hodgkins, S. B., Tyson, G., Sullivan, M. B., Brodie, E., Riley,
1323 W. J., Woodcroft, B., McCalley, C., Dominguez, S. C., Crill, P. M., Varner, R. K., Frolking, S., Cooper, W. T.,
1324 Chanton, J. P., Saleska, S. D., Rich, V. I., and Tfaily, M. M.: Plant organic matter inputs exert a strong control

- 1325 on soil organic matter decomposition in a thawing permafrost peatland, *Science of the Total Environment*, 820,
1326 152757, <https://doi.org/10.1016/j.scitotenv.2021.152757>, 2022.
- 1327 Wolter, J., Lantuit, H., Fritz, M., Macias-fauria, M., Myers-smith, I., Herzsuh, U., Wolter, J., and Wegener,
1328 A.: Vegetation composition and shrub extent on the Yukon coast , Canada , are strongly linked to ice-wedge
1329 polygon degradation, 1, 1–13, 2016.
- 1330 Wortel, M. T., Noor, E., Ferris, M., Bruggeman, F. J., and Liebermeister, W.: Metabolic enzyme cost explains
1331 variable trade-offs between microbial growth rate and yield, *PLOS Computational Biology*, 14, e1006010,
1332 <https://doi.org/10.1371/journal.pcbi.1006010>, 2018.
- 1333 Xu, S., Li, Z., Tang, W., Dai, Z., Zhou, L., Feng, T., Chen, M., Liu, S., Fu, X., Wu, T., Hu, E., and Yu, G.:
1334 MicrobiotaProcess: A comprehensive R package for managing and analyzing microbiome and other ecological
1335 data within the tidy framework, , <https://doi.org/10.21203/rs.3.rs-1284357/v1>, 2022.
- 1336 Xue, K., Yuan, M. M., Shi, Z. J., Qin, Y., Deng, Y., Cheng, L., Wu, L., He, Z., Van Nostrand, J. D., Bracho, R.,
1337 Natali, S., Schuur, E. A. G., Luo, C., Konstantinidis, K. T., Wang, Q., Cole, J. R., Tiedje, J. M., Luo, Y., and
1338 Zhou, J.: Tundra soil carbon is vulnerable to rapid microbial decomposition under climate warming, *Nature*
1339 *Climate Change*, 6, 595–600, <https://doi.org/10.1038/nclimate2940>, 2016.
- 1340 Zak, D. R. and Kling, G. W.: Microbial community composition and function across an arctic tundra landscape.,
1341 *Ecology*, 87, 1659–1670, [https://doi.org/10.1890/0012-9658\(2006\)87%255B1659:mccafa%255D2.0.co;2](https://doi.org/10.1890/0012-9658(2006)87%255B1659:mccafa%255D2.0.co;2), 2006.